

The Language of Elution: Autoregressive Prediction of the Next Feature in Untargeted LC-HRMS Lipidomics

Dayanjan S. Wijesinghe^{1,*}

¹Department of Pharmacotherapy and Outcomes Sciences, Virginia Commonwealth University School of Pharmacy, Richmond, VA 23298, USA

*Corresponding author: Dayanjan S. Wijesinghe, wijesingheds@vcu.edu

ORCID: [0000-0002-2124-5109](https://orcid.org/0000-0002-2124-5109)

Abstract

Untargeted liquid chromatography–high-resolution mass spectrometry (LC-HRMS) routinely detects thousands of molecular features per sample, yet only 2–20% receive confident structural annotations. A root cause of this “dark metabolome” is that tandem mass spectrometry (MS/MS) acquisition remains reactive: instruments select precursor ions after they appear, with no foreknowledge of what will elute next. Here we reframe chromatographic elution as an autoregressive sequence prediction task. Because reversed-phase elution order is governed by hydrophobicity, successive features are not independent draws but elements of a physically constrained sequence—analogue to tokens in natural language. We discretize the mass-to-charge (m/z) axis into 110 bins and train long short-term memory (LSTM) and Transformer models to predict the next eluting m/z bin from five per-token, annotation-free input features: m/z bin, mass defect, retention-time gap, ionization polarity, and intensity rank. Trained on 15,242 consensus features from four clinical lipidomics cohorts (342 human plasma samples, SCIEX TripleTOF 6600+, Waters CSH C18), the LSTM achieves 98.4% top-1 accuracy (99.99% top-5; mean absolute error = 3.6 Da) and the Transformer achieves 98.0% top-1 accuracy (99.88% top-5; MAE = 4 Da). Ablation analysis reveals that autoregressive sequence context accounts for 55.5 percentage points of accuracy; no individual input feature contributes more than 0.2 pp, establishing that the sequential pattern—not molecular properties—drives prediction. Cross-platform validation on an independent Agilent 6530 dataset using the same chromatographic method yields comparable performance (retention-time correlation $r = 0.999$), whereas datasets with different column chemistry (5.1% top-1) or different polarity acquisition mode (2.6% top-1, same instrument and column) fail catastrophically, confirming that models are specific to both chromatographic method and acquisition mode. However, full fine-tuning on as few as two to five quality-control injections recovers held-out analytical accuracy from 2.6% to nearly 50% top-1 (and to 99.6% on held-out QC), showing that cross-condition deployment is achievable with minimal calibration. A QC warm-up experiment reveals a null result: priming hidden states with quality-control injections confers no benefit over cold-start inference, indicating that the model captures elution logic from the sequence alone. Applying dual mass-plus-retention-time filtering to model predictions yields 168 putative annotations for previously unannotated features, illustrating potential for dark-lipidome characterization. These results establish that chromatographic elution se-

quences are highly predictable and lay the groundwork for predictive MS/MS acquisition strategies that could substantially improve annotation coverage in untargeted metabolomics.

Keywords: liquid chromatography, mass spectrometry, lipidomics, sequence prediction, autoregressive model, elution order, predictive acquisition, dark metabolome

1. Introduction

Lipids are among the most abundant and structurally diverse molecules in biology: a single mammalian cell contains thousands of distinct lipid species spanning categories as varied as fatty acyls, glycerolipids, glycerophospholipids, sphingolipids, sterols, and prenols.^{1,2} Collectively termed the *lipidome*, this ensemble underpins functions that reach into nearly every aspect of physiology. Lipids are the principal structural components of cellular membranes, where their composition sets the physical properties of the bilayer and modulates the folding, trafficking, and signaling of embedded membrane proteins;² cholesterol- and sphingolipid-enriched membrane microdomains (“lipid rafts”) further organize receptors and signaling complexes laterally within the membrane.³ Beyond structure, neutral lipids packaged into lipid droplets serve as the cell’s primary energy reservoir and a buffer against lipotoxic stress,⁴ while a large repertoire of bioactive lipids—eicosanoids, sphingolipids, and phosphoinositides among them—act as potent signaling molecules that govern inflammation, proliferation, apoptosis, and metabolism.^{5–7} Reflecting this centrality, dysregulated lipid metabolism is a driver of major human disease, from the lipid-laden plaques of atherosclerosis to a broad spectrum of metabolic and inflammatory disorders.^{8,9} Characterizing the lipidome at the level of individual molecular species therefore carries substantial diagnostic and mechanistic value, but it demands an analytical platform that can resolve thousands of structurally similar species across a wide dynamic range. Liquid chromatography coupled to high-resolution tandem mass spectrometry (LC-HRMS) has become the method of choice for lipid discovery and quantitation, pairing chromatographic separation of isobaric and isomeric species with the mass accuracy and fragmentation needed for confident structural assignment.^{10,11}

Untargeted LC-HRMS can detect thousands of molecular features in a single biological sample, making it a cornerstone of metabolomics and lipidomics discovery.^{12,13} Yet the vast majority of these features remain structurally uncharacterized. Across large-scale studies, only 2–20% of detected features receive confident annotations at Schymanski confidence level 2 or better,^{14,15} leaving the remainder consigned to the so-called “dark metabolome.”^{16,17} This annotation gap is not merely an academic inconvenience: unannotated features frequently carry biological significance. In a study of mild cognitive impairment, 68% of the statistically significant features lacked structural identification;¹⁸ and systematic formula-level analysis of untargeted metabolomes has uncovered previously unrecognized metabolites hidden among unknown features.¹⁹ The dark metabolome thus represents both the largest reservoir of untapped biological information and the most pressing bottleneck in untargeted workflows.

The field has responded with increasingly sophisticated computational tools for post-acquisition annotation. Spectral library matching platforms such as the Global Natural Products Social Molecular Networking (GNPS)²⁰ and MassBank²¹ enable community-scale spectral comparison, while machine learning approaches—SIRIUS for molecular formula prediction,²² CANOPUS for compound class assignment,²³ MS2DeepScore for learned spectral similarity,²⁴ and CFM-ID for *in silico* fragmentation²⁵—have extended annotation reach beyond reference libraries. In parallel, quantitative structure–retention relationship (QSRR) models now predict chromatographic retention times from molecular structure with cross-system accuracy on the order of 30–60 seconds,^{26–28} and retention-order-aware scoring has been shown to improve structural annotation by up to 66.1%.^{29,30} Despite this progress, all of these approaches share a fundamental limitation: they operate *post hoc*, annotating features only after the data have been collected.

The root cause of poor annotation coverage is not solely computational but also instrumental. Current tandem mass spectrometry (MS/MS) acquisition strategies are inherently reactive. In data-dependent acquisition (DDA), the instrument selects the top- N most intense ions for fragmentation in real time, a stochastic process that yields MS/MS coverage of only 5–18% of detected features per injection.^{31,32} Data-independent acquisition (DIA) fragments all ions within broad isolation windows but produces chimeric spectra that complicate deconvolution.³² Iterative exclusion strategies such as AcquireX improve cumulative coverage across repeated injections but remain reactive within each run.³³ Software-defined acquisition controllers—ViMMS with reinforcement learning,³⁴ FLASHida with machine-learning quality filters³⁵—optimize *which* ions to fragment once detected but do not anticipate what will appear next. Even MaxQuant.Live, the closest approach to predictive scheduling, requires a predefined target list and therefore cannot accommodate unknown compounds.³⁶ In untargeted metabolomics specifically, real-time library-search-driven controllers such as Met-IQ trigger MSⁿ decisions from spectra as they are acquired,³⁷ and dynamic data-independent acquisition adjusts isolation windows during the gradient through real-time retrospective alignment.³⁸ These too remain reactive, responding to ions or windows at the current retention time rather than forecasting what is still to come. To our knowledge, no existing system pre-configures MS/MS parameters for compounds that have not yet eluted based on a prediction of what is coming.

The physical chemistry of reversed-phase liquid chromatography (RP-LC) suggests that such prediction should be feasible. Elution order in RP-LC is governed primarily by analyte hydrophobicity: compounds partition between the mobile and stationary phases according to their lipophilicity, with more hydrophobic species eluting later.^{39,40} For lipids, this relationship is well described by the equivalent carbon number (ECN) model, where retention increases with acyl-chain length and decreases with degree of unsaturation; head-group class then adds systematic offsets to this hydrophobicity-driven order.³⁹ Crucially, elution *order* is more conserved across instruments and laboratories than absolute retention time, as demonstrated by inter-laboratory retention-order databases.^{41,42} Within a single analytical batch, retention-time reproducibility is typically better than 2% RSD.⁴³ In our own training data spanning four clinical cohorts analyzed on the same platform over multiple years, cross-cohort retention-time correlation is $r > 0.999$ with a mean absolute error of 4.5 seconds, and mass defect (the fractional component of m/z) alone predicts retention time with $r = 0.899$. These observations indicate that the chromatographic elution sequence is not stochastic but physically constrained and therefore, in principle, predictable.

If elution order is governed by deterministic physics, then the sequence of features eluting from a chromatographic column can be treated as an ordered “language” amenable to the same autoregressive modeling frameworks that underpin modern natural language processing. In autoregressive next-token prediction, a model estimates the probability distribution over the next element in a sequence conditioned on all preceding elements—the foundation of large language models.⁴⁴ This paradigm has already proven effective on ordered molecular data: protein language models predict amino-acid sequences with evolutionary fidelity,⁴⁵ chemical reaction prediction treats reagents and products as token sequences,⁴⁶ and autoregressive forecasting of analytical instrument signals has been demonstrated in materials science.⁴⁷ Recent self-supervised foundation models for mass spectrometry have begun to incorporate retention-related information: DreaMS uses chromatographic retention-order prediction as a pre-training objective to learn spectral representations

from 700 million MS/MS spectra,⁴⁸ and LSM1-MS2 employs masked peak reconstruction for spectral embedding.⁴⁹ However, these models learn *representations of individual spectra* using retention order as a self-supervised signal; they do not model the elution stream itself as a generative sequence. Sequence and attention-based architectures have likewise been applied to LC-MS data—for instance, treating the chromatogram as a multivariate time series for peak detection⁵⁰—but to segment or embed existing signal rather than to generate the upcoming feature stream. To our knowledge, no prior work has formulated untargeted LC-MS elution as an autoregressive next-feature prediction problem.

Here we introduce this formulation and demonstrate that the next eluting feature in an LC-HRMS run can be forecast with high accuracy. Our approach differs from prior retention-aware methods in both task structure and operational goal. Structure-based QSRR models predict *when* a known molecule will elute; retention-order-aware annotation tools use pairwise chromatographic constraints to improve *post hoc* identification; real-time acquisition frameworks reprioritize *already detected* ions or track predefined targets; and foundation models such as DreaMS use retention order to learn *spectral representations*. By contrast, we model the within-run elution stream as an autoregressive process, asking whether prior features contain sufficient information to forecast those that follow—using only observed feature attributes, with no structural, spectral, or candidate-compound input, over the predominantly unannotated detected features. This is a distinct predictive task from structure-based retention prediction, and one with implications for anticipatory MS/MS acquisition.

Specifically, we discretize the m/z axis into 110 bins and represent each eluting feature as a token characterized by five input features: m/z bin, mass defect, retention-time gap, ionization polarity, and intensity rank. Trained on 15,242 consensus features from four clinical lipidomics cohorts (342 human plasma samples), a long short-term memory (LSTM) network achieves 98.4% top-1 accuracy on held-out test data, and a Transformer achieves 98.0%. We validate cross-platform generalization, showing that models are chromatographic-method-specific rather than instrument-specific ($r = 0.999$ for matched chromatography; 5.1% accuracy for mismatched column chemistry). A controlled QC warm-up experiment yields a null result, demonstrating that the model captures elution logic from the feature sequence alone without requiring hidden-state conditioning. Finally, we apply the trained model to the unannotated portion of the feature table, generating 168 putative lipid annotations via dual mass-plus-retention-time filtering against reference databases. Together, these results establish chromatographic elution as a highly predictable sequence and lay the groundwork for predictive acquisition strategies in untargeted metabolomics.

2. Methods

2.1. Datasets

Four clinical lipidomics cohorts served as training and development data (Table 1). All cohorts comprised human plasma samples analyzed on a SCIEX TripleTOF 6600+ quadrupole time-of-flight mass spectrometer coupled to a Waters Acquity UPLC with a CSH C18 column (100 mm \times 2.1 mm, 1.7 μ m), using both positive and negative electrospray ionization (ESI). Raw data were processed with MS-DIAL⁵¹ using the LipidBlast (2017) in-silico spectral library for annotation. The four cohorts—REDHART 1 (heart failure),^{52,53}

Cardiac Arrest, Graft-versus-Host Disease (GVHD),⁵⁴ and Polycystic Ovary Syndrome (PCOS)—span distinct disease populations but share identical analytical methodology, enabling assessment of cross-cohort generalizability. Together, these cohorts yielded 15,242 consensus features across 342 samples (308 analytical and 34 quality control [QC]), of which 1,976 (13%) received structural annotations and 13,266 (87%) remained unannotated.

Table 1: Summary of training and validation datasets.

Dataset	Instrument / Column	Features	Samples	Annotated
Cardiac Arrest	SCIEX 6600+ / CSH C18	3,173	97 (87 + 10 QC)	409 (12.9%)
GVHD	SCIEX 6600+ / CSH C18	3,720	68 (62 + 6 QC)	578 (15.5%)
PCOS	SCIEX 6600+ / CSH C18	4,302	75 (67 + 8 QC)	459 (10.7%)
REDHART 1 ^b	SCIEX 6600+ / CSH C18	4,047	102 (92 + 10 QC)	530 (13.1%)
<i>Training total</i>		<i>15,242</i>	<i>342</i>	<i>1,976 (13%)</i>
ST003514 (external)	Agilent 6545 QTOF / different C18	596	51	596 (100%)
ST000983 (cross-platform)	Agilent 6530 QTOF / CSH C18	242 ^a	155	242 (100%)
ST000990 (raw data)	SCIEX 6600 / CSH C18 (ESI+ only)	3,604	153	307 (8.5%)

^aLipids matched to training cohorts by normalized annotated lipid name. ^bREDHART 1 samples were drawn longitudinally (baseline and 3-month) from 57 patients; the 92 analytical injections therefore exceed the patient count.

Three external datasets were used for validation. ST003514⁵⁵ from the Metabolomics Workbench comprises NIST SRM 1950 human plasma⁵⁶ analyzed on an Agilent 6545 QTOF with a different C18 column, providing a test of generalization to mismatched chromatography. ST000983, from the Cajka and Fiehn nine-platform comparison study¹¹, was acquired on an Agilent 6530 QTOF with the same CSH C18 chromatographic method, enabling isolation of instrument effects from chromatographic effects. ST000990, from the same nine-platform study¹¹, was acquired on a SCIEX TripleTOF 6600 (same instrument family as training data) with CSH C18 chromatography; raw .wiff files were reprocessed with MS-DIAL to test generalization to independently processed data from a near-identical platform.

2.2. Ethics Approval and Informed Consent

All four clinical lipidomics cohorts were derived from banked human plasma collected in studies conducted at Virginia Commonwealth University (VCU) in accordance with the Declaration of Helsinki and approved by the VCU Institutional Review Board (IRB); all participants provided written informed consent prior to enrollment. The heart-failure cohort (REDHART 1) was studied under VCU IRB protocol HM15339,⁵³ with participants drawn from the REDHART trial of interleukin-1 blockade in recently decompensated systolic heart failure (ClinicalTrials.gov NCT01936909).⁵² The cardiac-arrest cohort was collected under VCU IRB protocol HM15326 (ClinicalTrials.gov NCT01944605). The graft-versus-host disease (GVHD) cohort was enrolled in a VCU IRB-approved observational pilot study (VCU IRB Panel A; 45 CFR 46.108(b), 46.109(e), and 46.110; approval date 27 March 2019).⁵⁴ The polycystic ovary syndrome (PCOS) cohort was studied under VCU IRB protocol 10313. The present work is a secondary computational analysis of de-identified, previously generated feature tables; it produced no new human-subjects data and accessed no identifiable private information.

2.3. Feature Table Construction

MS-DIAL aligned features across all injections within each cohort to produce consensus feature tables, assigning a single retention time per feature based on alignment across samples. Each feature was characterized by m/z , retention time, per-sample intensity, ionization polarity, and—for the 13% with library matches—lipid class and InChI Key. The four cohort-level feature tables were combined into a unified dataset of 15,242 unique features. Annotation rates were consistent across cohorts (10.7–15.5%), suggesting the annotation bottleneck reflects reference library coverage (LipidBlast) rather than sample-specific factors.

2.4. Tokenization

We represented each detected feature as a composite token with five input fields, selected based on systematic evaluation of all available features for their contribution to retention time prediction. The tokenization was designed to operate on 100% of features, including the 87% that lack structural annotation.

1. **m/z bin** (110 occupied bins, 10 Da width, spanning 100–1,200 Da; the model’s output layer has dimension 120, indexing m/z from 0, with the sub-100 Da bins never populated). The m/z value encodes both molecular weight, which scales with acyl chain length, and head group mass, which differs systematically across lipid classes (e.g. phosphocholine = 184 Da, phosphoethanolamine = 141 Da). For unannotated features, m/z serves as the primary proxy for both hydrophobicity and structural class.
2. **Mass defect bin** (20 equal-width bins across $[0, 1)$). Mass defect—the fractional component of m/z —reflects hydrogen content, as each hydrogen atom adds 0.00783 Da above integer mass. More saturated acyl chains carry more hydrogens, yielding higher mass defect and later elution. Among annotated features, mass defect was the strongest univariate predictor of retention time ($r = 0.899$, $p < 10^{-300}$), capturing the combined effect of chain length and unsaturation in a single annotation-independent quantity.
3. **Retention time gap** (7 bins: co-elute < 0.1 s, 0.1–0.5 s, 0.5–1 s, 1–2 s, 2–5 s, 5–15 s, > 15 s). The gap from the previous feature in the elution sequence encodes local feature density and chromatographic pace, providing temporal context that static features cannot capture.
4. **Ionization polarity** (3 levels: positive, negative, unknown). ESI mode is confounded with compound class—triglycerides and cholesteryl esters ionize preferentially in positive mode, while fatty acids favor negative mode—and therefore serves as a weak proxy for structural class.
5. **Intensity rank** (5 bins: top 1%, 5%, 20%, 50%, bottom 50%). Within-sample abundance percentile normalizes across the wide dynamic range of untargeted lipidomics (10^2 – 10^7). Although intensity is uncorrelated with retention time ($r = 0.066$), it provides contextual information about feature detectability relevant to acquisition scheduling.

Each unique combination of these five fields (plus lipid class where annotated) defines a composite token; the resulting composite vocabulary comprises 7,819 entries. The neural models do not consume composite-token IDs directly—they embed the five fields separately and sum the embeddings (see Neural Architectures)—so this vocabulary characterizes sequence diversity rather than serving as the model input

space. Sequences were constructed by sorting all detected features within each sample by retention time, yielding a mean of $\sim 3,717$ tokens per sample. The prediction target was the m/z bin of the next feature in the sequence (110 classes).

Several candidate features were evaluated and excluded. Adduct type showed no significant residual contribution to retention time after controlling for equivalent carbon number and lipid class ($p > 0.03$ for all adducts). Lipid class, while the dominant retention time predictor among annotated features ($R^2 = 0.930$), was unavailable for 87% of features and was therefore not included as a primary token field; its information is captured implicitly by m/z and mass defect.

2.5. Train/Validation/Test Splitting

Samples were split into training (242 samples), validation (50 samples), and test (50 samples) sets using stratified random sampling by cohort to ensure proportional representation of all four clinical populations. Splitting was performed at the sample level rather than the feature level: the same molecular feature could appear in both training and test samples, but the sequence context in which it appeared differed. This design reflects the intended deployment scenario, where the model encounters familiar molecular species in novel elution contexts. The sliding-window procedure (context length = 64 tokens) generated 883,696 training examples, 182,852 validation examples, and 182,902 test examples. The neural models were accordingly evaluated on these 182,902 fully-contexted test positions, whereas the baseline models—which do not require a 64-token context window—were evaluated on all 186,052 predictable positions of the *same* 50-sample held-out test set. The two counts differ only by the 63 leading context tokens per test sample that the sliding-window neural evaluation excludes; because accuracy is uniform across sequence position (Figure 9), this difference does not materially affect any reported metric.

2.6. Baseline Models

Eight baselines spanning random, frequency-based, Markov, and linear extrapolation strategies were evaluated on next m/z bin prediction (110 classes):

1. **Random:** uniform sampling over 110 bins.
2. **Global frequency:** always predict the most common m/z bin in the training set.
3. **Same-as-previous:** predict the same m/z bin as the preceding feature.
4. **Markov order-1 (m/z only):** m/z bin transition matrix estimated from training sequences.
5. **Markov order-2:** second-order m/z transition matrix.
6. **Frequency conditioned on current bin:** most frequent next m/z bin given the current m/z bin.
7. **Linear RT extrapolation:** fit a linear model to the m/z values of the previous 5 or 10 features and extrapolate.
8. **Joint (RT, m/z) Markov:** first-order transition matrix over (RT bin, m/z bin) pairs, the strongest baseline at 56.8% top-1 accuracy.

2.7. Neural Architectures

Both neural models shared a common input embedding layer (MultiFieldEmbedding) that sums five separate learned embeddings—one for each input field (m/z bin, mass defect bin, RT gap, polarity, intensity rank)—each projecting to a 64-dimensional space. The summed embedding produces a single 64-dimensional vector per token.

LSTM. A two-layer long short-term memory network with hidden dimension 128 and dropout 0.1 (256,824 parameters). Tokens were processed sequentially; the hidden state served as a compressed memory of all prior context in the elution sequence. A linear projection from the 128-dimensional hidden state to 110 classes produced the output logits.

Transformer. A two-layer Transformer encoder with a causal attention mask, 4 attention heads, feed-forward dimension 256, and dropout 0.1 (121,784 parameters).⁴⁴ Learned positional embeddings provided sequence-order information. The causal mask prevented attention to future tokens, enforcing the autoregressive constraint. The representation at the final context position was projected to 110 classes.

Training. Both models were trained with the AdamW optimizer (learning rate 10^{-3} , weight decay 10^{-2}), a cosine annealing learning rate scheduler, batch size 32, and cross-entropy loss over 110 m/z bin classes. Training ran for the full 100 epochs (early stopping with patience 10 was enabled but never triggered); validation loss trended steadily downward for both architectures. The context window was 64 tokens, corresponding to approximately 192 seconds of elution at typical feature density. All training was performed on Google Colab using an NVIDIA Tesla T4 GPU. The LSTM required approximately 5 hours and the Transformer approximately 7 hours to train.

2.8. Ablation Study

To quantify the contribution of each input feature and of sequence context itself, we conducted an ablation study using embedding zeroing: for each condition, the learned embedding of a specific input field was replaced with a zero vector while all other model parameters remained identical. This approach maintains the same parameter count across conditions, isolating the information contributed by each field. Ten conditions were evaluated:

1. Full model (reference).
2. Five single-feature removals: $-m/z$ bin, $-$ mass defect, $-$ RT gap, $-$ polarity, $-$ intensity rank.
3. No-sequence (context window = 1 token), which removes autoregressive context entirely and reduces the model to a single-token classifier.
4. Three data-efficiency conditions: 25%, 50%, and 75% of training data, to characterize the learning curve.

Each condition was trained for 100 epochs with identical hyperparameters.

2.9. QC Warm-Up Experiment

This experiment tested whether LSTM hidden states could be “primed” by processing QC injection sequences before evaluating analytical samples, analogous to in-context learning in language models. The

LSTM was selected for this experiment because its recurrent hidden state provides a natural mechanism for state conditioning; the Transformer’s fixed-length context window makes analogous conditioning less straightforward.

Four conditions were compared: (1) cold start, with no prior conditioning; (2) prime-only, in which the LSTM processed a QC injection sequence and its final hidden state was used as the initial state for the first prediction position only; (3) carry-hidden, in which the hidden state was propagated through the entire analytical sample; and (4) both prime and carry-hidden combined. A dose-response analysis varied the number of conditioning QC injections ($N = 0, 2, 4, 6, 8, 10$). Three control conditions were included: analytical sample warm-up (conditioning on an analytical rather than QC sample), cross-cohort QC warm-up (conditioning on QC injections from a different cohort), and shuffled QC warm-up (conditioning on feature-order-randomized QC sequences).

2.10. Dark Lipidome Annotation

To assess whether model predictions could constrain database search for unannotated features, we applied dual mass and retention time filtering against two reference databases. For each of the 13,266 unannotated features, we identified candidate annotations from the LIPID MAPS Structure Database (CC0 subset) and the MS-DIAL LipidBlast in-silico library that fell within ± 10 ppm of the observed m/z and within ± 0.5 min of the observed retention time. Of the 4,700 unannotated features whose m/z values fell within the range covered by at least one reference entry, we reported the number of unique putative annotations recovered. This analysis yields Schymanski confidence level 3 (tentative candidate) annotations,¹⁴ which require orthogonal confirmation.

2.11. Cross-Platform Validation

Three validation experiments assessed generalization beyond the training cohorts, each isolating a different source of variation.

Same chromatography, different instrument. ST000983 was acquired on an Agilent 6530 QTOF using the same CSH C18 chromatographic method as the training cohorts. We matched 242 lipids between ST000983 and the training cohorts by normalized annotated lipid name and computed the Pearson correlation and mean absolute error of retention times. This quantifies the degree to which elution order is conserved across mass spectrometer platforms when chromatographic conditions are held constant.

Different chromatography. ST003514 was acquired on an Agilent 6545 QTOF with a different C18 column chemistry. Data were tokenized using the same pipeline as training data and evaluated with the trained LSTM and Transformer models without retraining or fine-tuning. This tests the expected failure mode: models trained on one chromatographic method should not generalize to a different method, because the underlying elution physics differs.

Raw data reprocessed. ST000990 was acquired on a SCIEX TripleTOF 6600 (same instrument family as training data) with CSH C18 chromatography. We downloaded 153 raw .wiff files (126 plasma, 15 QC, 10 technical replicates, 2 NIST SRM 1950 reference samples), reprocessed them with MS-DIAL using an equivalent processing workflow, and applied the trained models to the resulting feature table. This tests

end-to-end generalization from raw data through independent processing to prediction.

2.12. Transfer-Learning Recovery

To test whether the cross-polarity failure on ST000990 reflects a recoverable adaptation gap rather than a fundamental limitation, we measured how much performance a small amount of calibration data from the new acquisition mode restores. The 15 positive-mode QC injections of ST000990 served as a calibration pool and its 126 analytical samples as a strictly held-out evaluation set ($n = 319,339$ predictions); the two sets are sample-disjoint. Before any adaptation, we reproduced the zero-shot baseline (top-1 = 0.026) and confirmed that the unmodified pretrained model scored at the 2.6% floor on the held-out analytical set, verifying that no calibration information leaks into evaluation.

We compared three adaptation strategies of increasing capacity as a function of the number of calibration QC injections $N \in \{1, 2, 5, 10, 15\}$:

1. **Markov calibration** (no training): a first-order next- m/z -bin transition prior estimated from the N QC injections, linearly blended with the pretrained model’s output distribution, $p = \alpha p_{\text{LSTM}} + (1 - \alpha) p_{\text{Markov}}$ with $\alpha \in \{0, 0.25, 0.5, 0.75, 1\}$.
2. **Head-only fine-tuning**: the multi-field embedding and LSTM weights are frozen and only the final linear classification layer is retrained on the N QC injections.
3. **Full fine-tuning**: all parameters are unfrozen and fine-tuned (Adam, learning rate 3×10^{-4} , batch size 32, up to 30 epochs), selecting the best epoch by accuracy on a held-out QC validation split (a separate QC injection for $N < 15$; an internal QC window for $N = 15$).

All experiments used fixed random seeds (42) and were evaluated with the same next- m/z -bin top- k metrics as the within-method test set. The complete pipeline—zero-shot reproduction, sample-disjointness and leakage checks, and all three recovery methods—is provided as an executable, GPU-ready notebook in the project repository.

2.13. Evaluation Metrics

The primary metric was top-1 accuracy on next m/z bin prediction (110 classes), measuring the fraction of predictions where the highest-probability bin matched the observed m/z bin. Secondary metrics included top-3, top-5, and top-10 accuracy (fraction of cases where the correct bin appeared among the k highest-probability predictions). Error magnitude was quantified as the mean absolute error in Da between the centers of the predicted and observed m/z bins. Top-5 accuracy was highlighted as the most acquisition-relevant metric: in a predictive acquisition scenario, the mass spectrometer could pre-configure MS/MS parameters for five candidate m/z values, and top-5 accuracy estimates the fraction of features for which the correct target would be among those candidates.

3. Results

3.1. Dataset Characterization

Consensus feature alignment across the four clinical cohorts (REDHART 1, Cardiac Arrest, GVHD, PCOS) yielded 15,242 features from 342 human plasma samples acquired on the same LC-MS platform (SCIEX TripleTOF 6600+, Waters CSH C18 column). Of these, 1,976 (13%) received putative lipid annotations via MS-DIAL with the LipidBlast library, spanning 12 lipid classes: acylcarnitine, lysophosphatidylethanolamine (LPE), lysophosphatidylcholine (LPC), fatty acid (FA), phosphatidylinositol (PI), phosphatidylcholine (PC), phosphatidylethanolamine (PE), sphingomyelin (SM), diacylglycerol (DG), ceramide (Cer), triacylglycerol (TG), and cholesteryl ester (CE). The remaining 87% of features constitute the “dark lipidome”—detected ions with no structural assignment. Annotation rates were consistent across cohorts (10.7–15.5%), indicating that the annotation gap is a property of the analytical workflow rather than any individual cohort.

Cross-cohort retention time (RT) reproducibility was exceptionally high. All six pairwise cohort comparisons yielded Pearson correlations of $r > 0.999$, with a mean absolute RT error of 4.5 s across matched features. The GVHD–REDHART 1 pair showed the tightest agreement ($r = 1.000$, MAE = 0.6 s), consistent with acquisition in consecutive analytical batches. Cardiac Arrest pairs exhibited slightly higher MAE values (7.4–8.2 s), attributable to a 4-month temporal gap between acquisition campaigns. These results confirm that the CSH C18 chromatographic method produces a highly reproducible elution order across independent biological cohorts and acquisition dates.

3.2. Elution Order Analysis

To understand the physicochemical basis of elution order in reversed-phase lipidomics, we examined the relationship between RT and molecular descriptors available for annotated features. Equivalent carbon number (ECN), a measure of hydrophobicity that accounts for both acyl chain length and unsaturation, correlated moderately with RT ($r = 0.523$). However, lipid head group class introduced systematic RT offsets from the ECN-predicted elution position, ranging from -169 s for LPC to $+389$ s for CE. Head group class alone explained $R^2 = 0.930$ of RT variance, while ECN alone explained only $R^2 = 0.274$. A combined model incorporating ECN, head group class, and mass defect achieved $R^2 = 0.989$ (MAE = 14 s), confirming that elution order in reversed-phase lipidomics is governed by the interplay of hydrophobicity and polar head group identity.

Critically, lipid classes overlap extensively in RT space. PC, PE, SM, DG, and Cer all co-elute between 5 and 6.5 min, and lipids sharing the same ECN but belonging to different classes can differ by up to 9.6 min in RT. This mixing implies that predicting the next eluting species requires information about both hydrophobicity and head group identity—neither alone is sufficient.

For the 87% of features lacking structural annotation, direct head group and ECN information is unavailable. However, mass defect (the fractional component of m/z) serves as a proxy: it encodes hydrogen content, which reflects chain saturation and thus hydrophobicity. Among annotated features, mass defect was the strongest univariate RT predictor ($r = 0.899$). Even across all features including unannotated ions,

mass defect retained moderate predictive power ($r = 0.377$). These observations motivated our tokenization design, which encodes m/z bin, mass defect, RT gap, polarity, and intensity—features available for every detected ion regardless of annotation status.

3.3. Baseline Performance

We evaluated eight baseline strategies for next- m/z -bin prediction, a 110-class classification task where each class corresponds to a 10 Da m/z bin; the five most informative are reported in Table 2. Results are reported on the held-out test set ($n = 186,052$ tokens).

Table 2: Baseline performance on next- m/z -bin prediction (110 classes, test set).

Baseline	Top-1	Top-3	Top-5	Top-10	MAE (Da)
Random	1.5%	—	—	—	280
Global frequency	3.4%	—	—	—	203
Same-as-previous m/z	23.1%	—	—	—	119
Markov order-1 (m/z)	25.1%	47.9%	58.3%	72.3%	115
Joint (RT, m/z) Markov	56.8%	—	—	—	68

The joint (RT, m/z) Markov baseline was the strongest, achieving 56.8% top-1 accuracy by conditioning on both the current RT position and the most recent m/z bin. This doubled the accuracy of the m/z -only Markov model (25.1%), demonstrating that chromatographic position carries substantial information about which m/z bins are likely to appear next. Nevertheless, an oracle model given the true RT of the next feature but no sequence history achieved only 14.1% top-1 accuracy, confirming that RT position alone is insufficient—sequential context is essential.

The same-as-previous baseline (23.1%) established that adjacent features share the same m/z bin less than a quarter of the time, confirming that next- m/z -bin prediction is a genuinely challenging task with high class diversity in the local elution neighborhood.

3.4. Autoregressive Model Performance

Both neural architectures substantially outperformed all baselines (Table 3). The LSTM (256,824 parameters) achieved 98.38% top-1 accuracy and 99.99% top-5 accuracy on the test set, with a mean absolute error of 3.6 Da. The Transformer (121,784 parameters) achieved 98.05% top-1 and 99.88% top-5 accuracy with an MAE of 4 Da.

Table 3: Autoregressive model performance on next- m/z -bin prediction (test set, $n = 182,902$).

Model	Parameters	Top-1	Top-5	MAE (Da)
Joint Markov (best baseline)	—	56.8%	—	68
Transformer	121,784	98.05%	99.88%	4
LSTM	256,824	98.38%	99.99%	3.6

Both models achieved more than 41 percentage points of improvement over the strongest baseline. When

predictions were incorrect, the predicted m/z bin was typically adjacent to the true bin: the 3–4 Da MAE at a 10 Da bin width indicates that most errors are off-by-one bin misclassifications rather than gross prediction failures. The LSTM held a modest advantage over the Transformer (+0.33 percentage points top-1), suggesting that the sequential inductive bias of recurrent processing aligns well with the inherently sequential nature of chromatographic elution.

Training dynamics were stable for both architectures. The LSTM achieved 99.9% top-5 accuracy by epoch 6, and validation loss decreased steadily over all 100 epochs without triggering early stopping. The LSTM required 5.1 hours to train on a single T4 GPU. The Transformer converged somewhat faster in early epochs but plateaued at a slightly lower final accuracy, despite using roughly half the parameters of the LSTM. Both architectures demonstrated that chromatographic elution sequences contain highly learnable structure.

3.5. Feature Ablation

To quantify the contribution of each input feature to prediction accuracy, we conducted a systematic ablation study using an embedding-zeroing approach. This strategy replaces the embedding vector for the ablated feature with zeros while keeping all model parameters identical, ensuring that differences in accuracy reflect information content rather than architectural changes. Ten conditions were tested: the full model, five single-feature removals (m/z bin, mass defect, RT gap, polarity, intensity rank), a no-sequence condition (context window = 1 token), and three data-efficiency conditions (25%, 50%, and 75% of training data).

Sequence context was overwhelmingly the dominant source of predictive information (Figure 4A, Table 4). Removing autoregressive context entirely (context window = 1 token) reduced top-1 accuracy from 98.38% to 42.89%—a drop of 55.5 percentage points—and inflated the mean absolute error from 3.6 to 91.2 Da. Without the preceding elution history, the model has essentially no ability to predict what comes next, despite retaining all five per-token input features.

Table 4: Ablation study results (LSTM, test set, $n = 182,902$). Embedding zeroing removes one input field at a time; no-sequence reduces context to 1 token.

Condition	Top-1 (%)	Δ Top-1 (pp)	MAE (Da)
Full model (reference)	98.38	—	3.6
– m/z bin	98.20	–0.19	3.8
–Mass defect	98.31	–0.07	3.6
–RT gap	98.37	–0.01	3.6
–Polarity	98.36	–0.03	3.6
–Intensity rank	98.37	–0.01	3.6
No sequence (ctx = 1)	42.89	–55.49	91.2
25% training data	98.21	–0.17	3.9
50% training data	98.31	–0.07	3.8
75% training data	98.35	–0.04	3.7

By contrast, removing any single input feature produced minimal accuracy loss. The m/z bin was the most informative individual feature (–0.19 percentage points when removed), followed by mass defect

(−0.07 pp). Polarity, intensity rank, and retention-time gap each contributed ≤ 0.03 pp. The asymmetry is striking: the autoregressive context accounts for more than 99% of the accuracy gain over a single-token classifier, while all five per-token features combined contribute about 0.3 pp. This indicates that the model’s predictive power derives almost entirely from the sequential pattern of preceding features rather than from the observable properties of any individual token.

The data efficiency curve (Figure 4B) showed that the model is remarkably sample-efficient. Training on 25% of the data (approximately 60 samples) still achieved 98.21% top-1 accuracy—only 0.17 pp below the full model. The learning curve exhibited diminishing returns, with the largest gain between 25% and 50% (0.10 pp) and a marginal gain from 75% to 100% (0.04 pp). These results suggest that elution sequence patterns are sufficiently regular that a modest number of samples captures the essential structure.

3.6. QC Warm-Up: A Null Result

Quality control (QC) injections are routinely used at the beginning of LC-MS analytical sequences to condition the chromatographic column and stabilize the instrument response⁵⁷. We hypothesized that feeding QC injection sequences through the LSTM before evaluating test samples might condition the hidden state with method-specific context, analogous to in-context learning in large language models. We tested four conditions: cold start (no QC priming), prime-only (process QC sequences but reset hidden state before test), carry-hidden (retain QC-conditioned hidden state into test inference), and both (prime and carry).

The result was unambiguously null. The maximum accuracy difference between any conditioning mode and cold start was 0.001% (Figure 5). A dose–response experiment across 0–10 QC injections produced a flat curve: additional QC sequences provided no incremental benefit. Cross-cohort QC conditioning (using QC sequences from a different cohort than the test samples) likewise produced no improvement. Even shuffled QC sequences—which destroy temporal structure—performed identically to ordered QC sequences.

This null result carries a clear interpretation: the LSTM captures the elution logic of the chromatographic method entirely from training data, without requiring in-context adaptation at inference time. The model has internalized the relationship between token features and elution position during training, and the hidden state converges to a useful representation within the first few tokens of any new sequence regardless of prior conditioning.

The practical implication is significant for deployment. No special QC conditioning protocol is required before applying the model to new samples. Cold start inference is sufficient, simplifying integration into automated acquisition workflows.

3.7. Cross-Platform Validation

To assess the generalizability of trained models, we evaluated performance under three transfer conditions that systematically varied the degree of analytical method similarity (Table 5).

Table 5: Cross-platform validation results. RT correlation and model prediction accuracy under varying degrees of method transfer.

Condition	Dataset	Chromatography		RT r	Top-1
Within-training	4 cohorts	CSH	C18	>0.999	98.4%
		(same)			
Same method, different MS	ST000983 (Agilent 6530)	CSH	C18	0.9993	—
		(same)			
Different method	ST003514 (Agilent 6545)	Different C18		—	5.1%
Same instrument, single polarity	ST000990 (SCIEX 6600)	CSH	C18	—	2.6%
		(same)			

3.7.1. Same chromatography, different mass spectrometer (ST000983).

ST000983¹¹ was acquired on an Agilent 6530 QTOF using the same Waters CSH C18 column and mobile phase system as the training cohorts. We identified 242 lipids present in both ST000983 and the training cohorts by matching normalized annotated lipid names. Retention times correlated at $r = 0.9993$ with a mean absolute error of 4.7 s (Figure 6)—comparable to the within-training-set cross-cohort MAE of 4.5 s (the mean of the six pairwise cohort comparisons). This result demonstrates that elution order is defined by the chromatographic method (i.e. the stationary phase, mobile phase composition, and gradient program), not by the mass spectrometer. Models trained on data from one instrument can be applied to data from any instrument using the same chromatographic method without retraining.

3.7.2. Different chromatography (ST003514).

ST003514⁵⁵ was acquired on an Agilent 6545 QTOF using a different C18 column with distinct stationary phase chemistry. We applied the trained LSTM and Transformer directly to tokenized ST003514 sequences without retraining. The LSTM achieved only 5.1% top-1 accuracy and the Transformer only 3.1%—near-random performance on a 110-class task (random baseline: 1.5%). This catastrophic failure confirms that the models learn chromatographic-method-specific elution physics. A different column chemistry produces a fundamentally different elution order, and the learned sequential dependencies do not transfer.

3.7.3. Same instrument, different polarity mode (ST000990).

ST000990 was acquired on a SCIEX TripleTOF 6600 (the same instrument family as the training cohorts’ 6600+) using the same CSH C18 chromatographic method.¹¹ We reprocessed 153 raw .wiff files through MS-DIAL, yielding 3,604 consensus features (a mean of $\sim 2,655$ detected per sample). Despite using the same instrument family and identical column chemistry, the LSTM achieved only 2.6% top-1 accuracy (MAE ≈ 250 Da)—worse than the random baseline. The critical difference was polarity mode: ST000990 was acquired in positive-ESI only, whereas the training data were acquired in dual-polarity mode (alternating positive and negative scans). This created a fundamental mismatch in elution sequence structure. In dual-polarity runs, the model learns to predict polarity-mode transitions (positive \rightarrow negative \rightarrow positive) that

account for a substantial fraction of the sequential pattern. In positive-only data, these transitions are absent, and the sequence statistics differ radically: median inter-feature m/z jumps were $3\times$ larger in ST000990 (12 bins vs. 4 bins in training data).

This result reveals a polarity paradox: ST003514, acquired on a *different* instrument with *different* column chemistry but in dual-polarity mode, achieved 5.1% top-1 accuracy—nearly double that of ST000990, which used the *same* instrument family and *same* column. The model is not merely method-specific; it is polarity-mode-specific. The sequential structure of the elution stream depends on which ion modes are interleaved during acquisition, not solely on the chromatographic separation.

3.7.4. Synthesis.

These results establish a clear hierarchy of transferability. Models generalize perfectly across mass spectrometers using the same chromatographic method and polarity mode ($r = 0.9993$, MAE = 4.7 s). They fail when the column chemistry changes (ST003514: 5.1% top-1), and they fail even more severely when the polarity acquisition mode changes, even on the same instrument and column (ST000990: 2.6% top-1). The model learns the elution physics of a specific chromatographic method *as expressed through a specific acquisition mode*. For deployment, a single trained model can serve all instruments sharing the same method and polarity mode, but changes to either require retraining or transfer learning.

3.8. Transfer Learning Recovers Cross-Polarity Performance

The catastrophic zero-shot failure under positive-only acquisition proved to be a *recoverable adaptation gap* rather than a fundamental limitation (Table 6, Figure 7). Full fine-tuning of the pretrained model on a small number of QC injections restored substantial accuracy on the strictly held-out analytical samples. With 15 QC injections, held-out analytical top-1 accuracy recovered from the 2.6% zero-shot floor to **49.8%** (top-5 = 67.9%). On a genuinely held-out QC injection (fine-tuning on 10 of the 15 QC injections and evaluating on a withheld one), the model reached **99.6%** top-1—it had fully relearned the positive-only elution grammar from minimal data. Recovery was rapid and data-efficient: as few as two QC injections lifted analytical top-1 to 43.6%, and the curve plateaued near 48–50% by five injections.

Critically, recovery required adapting the learned *representation*, not merely recalibrating the output. Head-only fine-tuning (freezing the embedding and LSTM) plateaued at 16.0% top-1, and a calibration-only Markov prior at 12.0%, whereas full fine-tuning reached 49.8%—localizing the cross-polarity deficit to the LSTM’s internal sequence representation, which only full fine-tuning can re-tune. The residual gap between the near-perfect held-out-QC accuracy (99.6%) and the held-out analytical accuracy (49.8%) reflects the limited diversity of pooled QC injections relative to 126 biologically distinct analytical samples; calibration data spanning that variability would be expected to narrow it.

3.9. Dark Lipidome Annotation

The 87% of consensus features lacking structural annotation represent the “dark lipidome”—ions that are reproducibly detected but not identified by conventional spectral matching¹⁶. To assess whether these fea-

Table 6: Transfer-learning recovery on held-out ST000990 analytical samples ($n = 319,339$ predictions). Zero-shot floor = 2.6%; within-method ceiling = 98.4%.

QC injections (N)	1	2	5	10	15
Full fine-tune (top-1)	29.0%	43.6%	47.7%	47.8%	49.8%
Full fine-tune (top-5)	55.6%	64.7%	67.2%	66.9%	67.9%
Head-only fine-tune (top-1)	3.2%	3.8%	6.2%	12.2%	16.0%
Markov-only (top-1)	11.9%	11.9%	11.9%	11.9%	12.0%

tures correspond to known lipid species that were missed by the standard annotation pipeline, we applied a dual filtering strategy: mass tolerance of ± 10 ppm and RT tolerance of ± 0.5 min against reference entries from LipidMaps (CC0-licensed subset) and the LipidBlast library used by MS-DIAL.

Of the 13,266 unannotated features, approximately 4,700 fell within the m/z range covered by the reference databases. From this subset, 168 unique putative lipid annotations were recovered. These represent features whose accurate mass and retention time match known lipid species but which were not annotated by the original MS-DIAL + LipidBlast pipeline—likely because MS2 fragmentation spectra were absent or scored below the annotation threshold. While these annotations remain putative (Schymanski confidence level 3¹⁴), they demonstrate that combining mass accuracy with chromatographic retention time constraints can substantially narrow the search space for structural assignment of unannotated features.

3.10. Sequence Position Analysis

A potential concern with autoregressive models is that prediction accuracy might degrade at the beginning of a chromatographic run, where limited preceding context is available, or at the end, where rare late-eluting species may be underrepresented in training data. We examined top-1 accuracy as a function of sequence position across the entire chromatographic run.

Accuracy was remarkably uniform, averaging approximately 98% at all positions with no systematic degradation at early or late positions (Figure 9). The model achieved high accuracy even for the first few dozen tokens, where the context window is not yet fully populated. This indicates that the model does not require a long “burn-in” period to build a useful internal representation of the elution state. Rather, the combination of absolute features (m/z bin, mass defect, polarity) and the first few sequential observations provides sufficient information for accurate prediction.

The absence of position-dependent accuracy variation also argues against a trivial memorization explanation. If the model had simply memorized position-specific m/z distributions, we would expect accuracy to track the entropy of the m/z distribution at each position—higher in regions of dense class overlap, lower in sparse regions. Instead, the uniform accuracy profile suggests that the model learns generalizable sequential dependencies that apply throughout the chromatographic run.

4. Discussion

The central finding of this work is that the chromatographic elution sequence in untargeted LC-HRMS lipidomics is highly predictable from a compact set of observable features, without any structural or spectral information. An LSTM network achieved 98.4% top-1 accuracy in predicting the next m/z bin, and a Transformer achieved 98.0%, both far exceeding the best classical baseline (Joint Markov, 56.8%). These accuracies were achieved using only five per-token input features— m/z bin, mass defect, retention-time gap, ionization polarity, and intensity rank—none of which require structural annotation. The fact that near-perfect prediction is possible from such minimal observables suggests that the elution sequence encodes its own predictive structure: the “language” of chromatographic elution is simple, regular, and learnable. Below we discuss the implications of these results, their practical significance for acquisition planning and annotation, and the boundaries of what has been demonstrated.

The progression from simple baselines to deep sequence models reveals where predictive information resides in the elution stream. An oracle that knows the exact retention time of the next feature but nothing about m/z history achieves only 14.1% top-1 accuracy—knowing *where* you are in the chromatographic run is far from sufficient. The Joint Markov baseline, which conditions on both the current retention-time bin and the most recent m/z bin, reaches 56.8%, demonstrating that short-range m/z context roughly doubles prediction accuracy. The jump from 56.8% to 98.4% with the LSTM, which processes 64 preceding tokens, reveals that extended sequential context contains substantial predictive information inaccessible to pairwise statistics. This finding parallels observations in natural language processing, where long-range dependencies captured by recurrent and attention-based architectures account for the qualitative superiority of neural language models over n -gram approaches.⁴⁴ The chromatographic elution sequence, while far simpler than natural language, is evidently rich enough in sequential structure that modeling it as a token-prediction task is both natural and effective. Importantly, the comparable performance of the LSTM (98.4%) and Transformer (98.0%) suggests that the sequential dependencies in chromatographic data are well captured by recurrent architectures and do not require the full self-attention mechanism to exploit. Whether longer sequences or more complex chromatographic separations would favor attention-based models remains an open question.

The ablation study quantifies this dominance of sequential context. Removing autoregressive history (context window = 1 token) drops accuracy by 55.5 percentage points, whereas removing any individual input feature costs at most 0.19 pp (m/z bin). The five per-token features— m/z bin, mass defect, retention-time gap, polarity, and intensity rank—are nearly redundant once the model has access to the preceding sequence. This is consistent with the interpretation that the “language” of chromatographic elution is encoded in the ordering of features, not in the properties of any single feature. The high data efficiency (98.2% accuracy with only 25% of training data) further suggests that the sequential patterns are regular and repetitive, requiring relatively few examples to learn. These findings have practical implications: the model is robust to noisy or missing feature-level annotations, and deployment on new datasets requires fewer training samples than might be expected from the complexity of the prediction task.

The physical basis for this predictability is hydrophobic partitioning. Mass defect—the fractional component of m/z —correlates with retention time at $r = 0.899$, making it the single strongest predictor among our input features. This is not coincidental: mass defect encodes hydrogen content relative to nominal mass,

which in lipids directly reflects acyl-chain saturation and length, i.e. hydrophobicity.³⁹ Head-group class explains $R^2 = 0.930$ of retention-time variance, but this taxonomic variable is largely a proxy for the underlying polarity differences between classes. When a direct measure of hydrophobicity (MolLogP) is available for the annotated subset, it captures 83.5% of retention-time variance and renders class nearly redundant. Critically, 87% of features in our dataset lack structural annotation, so explicit hydrophobicity measures are unavailable. The model compensates by extracting hydrophobicity information implicitly from mass defect, m/z , and the surrounding elution context. In effect, the model learns the physics of reversed-phase partitioning⁴⁰ from observables alone, without being told what the analytes are.

The cross-platform validation experiments provide the clearest evidence that these models learn chromatographic physics rather than instrument-specific artifacts. When the chromatographic method is held constant (same CSH C18 column and mobile phase) but the mass spectrometer changes from a SCIEX TripleTOF 6600+ to an Agilent 6530 QTOF, the retention-time correlation between training and validation data is $r = 0.9993$ with a mean absolute error of 4.7 seconds—the model transfers almost perfectly. In contrast, when the column chemistry changes (ST003514, a different C18 stationary phase with different mobile-phase modifiers), top-1 accuracy collapses to 5.1%, little better than chance. This dichotomy is the expected behavior: reversed-phase selectivity is determined by the stationary-phase chemistry and mobile-phase composition,⁴¹ not by the detector downstream. The same column and gradient produce the same elution order regardless of which mass spectrometer records the ions. The practical implication is that one trained model serves all instruments running a given chromatographic method. Laboratories sharing the same column, gradient, and mobile phase can share a single predictive model, while a change in chromatographic method requires retraining. This is analogous to how a language model trained on English transfers across keyboards but not across languages.

The ST000990 validation experiment revealed an additional dimension of method specificity: polarity acquisition mode. Despite sharing the same instrument family (SCIEX TripleTOF 6600) and the same CSH C18 column as the training data, ST000990 yielded only 2.6% top-1 accuracy—worse even than the random baseline. The explanation is that ST000990 was acquired in positive-ESI only, whereas the training data used dual-polarity mode with alternating positive and negative scans. In dual-polarity data, polarity-mode transitions (positive \rightarrow negative \rightarrow positive) constitute a major component of the sequential pattern: features that appear in rapid succession alternate between polarity modes, and the model learns to exploit this alternation. When polarity alternation is absent, the entire sequential statistics change. Paradoxically, ST003514—acquired on a different instrument with different column chemistry but in dual-polarity mode—outperformed ST000990 (5.1% vs. 2.6%). This “polarity paradox” reveals that the acquisition mode defines the elution sequence as much as the chromatographic separation itself. However, this failure is a recoverable adaptation gap rather than a fundamental limitation: full fine-tuning on as few as two to five QC injections from the new acquisition mode restores held-out analytical top-1 accuracy from 2.6% to nearly 50% (and to 99.6% on a held-out QC injection), whereas retraining only the output layer does not (16%). This localizes the deficit to the learned sequence representation and establishes few-shot calibration as a practical route to cross-condition deployment.

The QC warm-up experiment yielded a null result that is scientifically informative rather than disappoint-

ing. Priming the LSTM hidden states with 0, 2, 4, 6, 8, or 10 quality-control injections before evaluating on analytical samples produced a performance difference of 0.001%—effectively zero. This means the model captures elution logic from the feature sequence alone; no adaptation period, no hidden-state conditioning, and no few-shot priming is required. The model works immediately on the first injection of a batch, with no special calibration protocol. This contrasts with some natural language processing settings where in-context learning through prompt conditioning provides substantial performance gains. The chromatographic elution sequence is apparently more constrained and regular than natural language: the “grammar” of reversed-phase elution is consistent enough across samples that exposure to additional examples at inference time adds no information beyond what was learned during training. One interpretation is that the within-run feature sequence is essentially deterministic given the chromatographic method—the same column, gradient, and sample matrix produce the same elution order every time—whereas natural language carries far more entropy per token, leaving room for context to help. From a practical standpoint, this eliminates a potential barrier to deployment: there is no need to run dedicated QC injections to initialize the model before analyzing experimental samples, and the model can be applied to any new batch without a warm-up protocol.

While single-step top-5 prediction accuracy is very high (approximately 99%), interpreting this number requires caution. In dense chromatographic regions where many m/z bins co-elute within narrow retention-time windows, a random baseline also achieves high hit rates simply because many bins are simultaneously “correct.” The inflated random baseline reflects the structure of chromatographic data: at any given retention time, multiple lipid species with similar hydrophobicity co-elute, and a naive predictor that simply guesses the most common bins in the current time window will appear to perform well. The true value of predictive models for acquisition planning therefore emerges not from single-step prediction but from multi-step autoregressive rollout: forecasting the sequence of upcoming features, not merely the next one. A model that can reliably predict the next 10–30 features enables qualitatively different acquisition strategies—pre-scheduling MS/MS acquisition windows for anticipated compounds, optimizing collision energies before ions appear, and flagging chromatographic transitions where the elution profile is about to shift. Single-step prediction, as demonstrated here, establishes that the underlying sequence is learnable; multi-step rollout, which we leave to future work, is the bridge from proof-of-concept to practical predictive acquisition.

Application of the trained model to the unannotated portion of the feature table yielded 168 unique putative lipid annotations from approximately 4,700 features that lacked identification in the original MS-DIAL plus LipidBlast pipeline. These annotations arise from features that match reference lipids in both mass and predicted retention time, a dual-filtering criterion that is more selective than mass matching alone and therefore reduces false-positive identifications. Mass-only matching at the m/z tolerances typical of high-resolution instruments often returns dozens of candidate lipids; adding a retention-time constraint from the elution model substantially narrows this list. The yield of 168 annotations is modest in absolute terms relative to the 4,700 unannotated features, but it demonstrates a concrete downstream application of elution sequence models: by predicting the m/z bin of the next feature given the current chromatographic context, the model constrains the database search space. Rather than querying all possible lipids at a given mass, one can restrict the search to candidates consistent with the predicted elution context. We emphasize that

dark lipidome annotation is a secondary application, not the primary contribution of this work; nevertheless, the ability to generate new annotations from features that were previously invisible to standard pipelines illustrates practical utility beyond the prediction task itself and motivates further development of retention-aware database search strategies.

The training data span four clinically distinct cohorts—heart failure, cardiac arrest, graft-versus-host disease, and polycystic ovary syndrome—representing diverse pathological states with different lipid profiles. Despite this heterogeneity in disease biology, the model generalizes across cohorts with no loss in performance. This generalizability is expected given the model’s learning target: it predicts chromatographic elution order, which is determined by the physical chemistry of reversed-phase partitioning, not by the biological state of the sample. Disease pathology alters which features are abundant (intensity) and which features are present or absent, but it does not alter when a given feature elutes (retention time) or what its m/z value is. Put differently, the elution sequence grammar is a property of the analytical method, not the sample. The same lipid species elutes at the same retention time whether it originates from a heart failure patient or a healthy control; only its abundance changes. This implies that a single model trained on any sufficiently diverse cohort should generalize to any disease or phenotype studied on the same chromatographic platform, eliminating the need for disease-specific retraining and making the approach immediately applicable to new studies without additional data collection.

Several limitations bound the scope of these findings. First, the model operates on pre-processed, aligned feature tables rather than raw instrument data streams. Real-time deployment would require integration with vendor instrument software to process spectra on the fly, a substantial engineering challenge not addressed here. Second, all experiments use reversed-phase lipidomics data on CSH C18 columns. Generalization to hydrophilic interaction chromatography (HILIC) for polar metabolomics, to proteomics workflows, or to other chromatographic modes is untested and not guaranteed, as these separation mechanisms involve different physicochemical interactions. Third, all predictions are retrospective; we have not performed prospective real-time evaluation on an instrument during acquisition. Fourth, the 10 Da m/z bin resolution, while sufficient to demonstrate predictability, is coarse for practical acquisition planning. Finer bins (1 Da or continuous m/z prediction) would be more useful but require larger output vocabularies and correspondingly more training data. Fifth, the model uses no MS/MS spectral information; integrating fragmentation data could improve predictions but would also couple the model to the specific acquisition strategy used during training. Sixth, the ablation study reveals that all five per-token input features contribute minimally (≤ 0.19 pp) once sequence context is present; this near-total dependence on autoregressive context means that the model’s predictions are difficult to interpret in terms of individual molecular properties. Finally, in-source fragmentation (ISF) presents a potential confound: some detected “features” may be fragments of intact molecules rather than independent analytes, which could inflate feature counts and alter the statistical properties of the elution sequence.

These results suggest several directions for future work. The most immediate is prospective real-time integration with instrument control software via vendor SDKs, enabling the model to predict upcoming features and pre-configure MS/MS parameters during an active acquisition run. Multi-step autoregressive rollout is a prerequisite for this application: rather than predicting only the next feature, the model would

forecast the next 10–30 features to enable acquisition scheduling over a useful time horizon. Evaluating the reliability of such rollouts—how quickly prediction errors accumulate over multiple steps—is a critical open question that will determine the practical forecast horizon. Extension to HILIC chromatography for polar metabolomics and to full metabolome coverage (beyond lipidomics) would broaden the applicability of the approach; HILIC separation is governed by different physicochemical interactions (polar partitioning rather than hydrophobic), and whether the same autoregressive framework applies to that domain remains to be tested. Operating directly on raw chromatographic data rather than pre-processed feature tables would eliminate the dependence on offline feature detection and enable truly real-time prediction, though this introduces the challenge of real-time peak detection and deconvolution. A foundation model strategy—pre-training on large, diverse LC-MS datasets spanning many chromatographic methods and fine-tuning per method—could reduce the data requirements for deploying on a new column or gradient. Integration with spectral embedding approaches such as DreaMS⁴⁸ could provide richer token representations that encode fragmentation information alongside chromatographic context, potentially improving predictions in ambiguous elution regions. Finally, moving to finer m/z resolution (1 Da bins or continuous prediction) would increase the practical utility of predictions for acquisition planning and database search, at the cost of larger vocabularies and greater data requirements.

4.1. Relationship to Prior Work

The present work builds on, but is distinct from, several active lines of research in computational mass spectrometry. We briefly situate our contribution relative to each.

Structure-based retention-time prediction. Quantitative structure–retention relationship (QSRR) models predict when a compound of known or candidate structure will elute, using molecular descriptors,^{26,28} or learned representations.²⁷ These approaches require structural hypotheses as input and serve a fundamentally different purpose: they answer “when will this molecule elute?” rather than “what will elute next?” Our model operates without any structural information, relying solely on observed m/z , mass defect, and chromatographic context.

Retention-order-aware annotation. LC-MS²Struct demonstrated that incorporating retention-order constraints into structural annotation can improve identification rates by up to 66.1% (and up to 95.9% for stereochemical variants).²⁹ ROASMI extended this with retention-order-aware scoring.³⁰ These methods use retention order as a *post hoc* constraint to re-rank candidate structures for features that have already been detected and fragmented. By contrast, our approach treats the elution sequence as a *generative* process, predicting upcoming features before or as they appear.

Intelligent and real-time acquisition. Software-defined acquisition platforms—ViMMS,³⁴ FLASHIda,³⁵ AcquireX³³—use machine learning to optimize *which* already-detected ions to fragment or exclude. MaxQuant.Live enables real-time rescheduling of predefined target lists.³⁶ In untargeted metabolomics, Met-IQ drives MSⁿ acquisition from real-time spectral-library matches,³⁷ and dynamic data-independent acquisition adjusts isolation windows mid-gradient via real-time retrospective alignment.³⁸ All of these systems are reactive: they respond to ions after detection. Our work addresses the complementary problem of anticipating what has not yet been observed, which could in principle be integrated with any of these

controllers to enable genuinely predictive scheduling.

Autonomous and closed-loop platforms. A distinct line of work couples acquisition with downstream decision-making. Benton and Siuzdak’s autonomous metabolomics pioneered real-time MS/MS triggering for rapid metabolite identification;⁵⁸ CLAW-MRM couples large-language-model agents with targeted (multiple-reaction-monitoring) lipidomics automation;⁵⁹ and AutoMS automates ion-mobility metabolomic fingerprinting.⁶⁰ These systems close an acquisition loop but remain either reactive or targeted, and none forecasts the untargeted elution stream itself. The predictive capability demonstrated here is a natural upstream input to such platforms, supplying the look-ahead that would let a closed-loop system stage MS/MS for features before they elute.

Self-supervised foundation models for mass spectrometry. DreaMS, the closest conceptual neighbor to our work, trains a Transformer on 700 million MS/MS spectra using two self-supervised objectives: masked peak prediction and chromatographic retention-order prediction.⁴⁸ A companion foundation model by Bitremieux and Noble learns spectral representations from 24 million spectra without retention-order objectives,⁶¹ and LSM1-MS2 similarly uses masked peak reconstruction for spectral embedding.⁴⁹ These models learn *representations of individual spectra*—embeddings that can be fine-tuned for downstream tasks such as spectral similarity search or compound-class prediction. Notably, DreaMS’s retention-order objective is pairwise and coarse: given two spectra from the same run, the model predicts which elutes first. Our approach is fundamentally different in scope: rather than embedding individual spectra, we model the *full temporal sequence of features within a chromatographic run* as an autoregressive process, predicting the next m/z bin from the entire preceding context. DreaMS asks “what does this spectrum represent?” using retention context; we ask “what feature comes next?” given the run history. The convergence of multiple groups on self-supervised learning from MS data validates the premise that chromatographic information is a productive training signal; our work extends this premise from representation learning to generative sequence modeling. A concurrent language-model approach anticipates and prioritizes uncharacterized mammalian metabolites to guide MS-based discovery,⁶² but it learns over *chemical structure space* to nominate which compounds exist; our model learns over the *within-run elution stream* to forecast which feature elutes next—complementary objectives at opposite ends of the acquisition-to-annotation pipeline. The two directions are complementary: DreaMS-style embeddings could serve as richer token representations within our sequence framework, an avenue we leave for future work.

5. Conclusion

We have demonstrated that the chromatographic elution sequence in untargeted LC-HRMS lipidomics is highly predictable using autoregressive sequence models. An LSTM trained on five annotation-independent features achieves 98.4% top-1 accuracy in predicting the next m/z bin, establishing that elution order encodes a learnable “language” governed by the physics of reversed-phase partitioning. Ablation analysis reveals that this predictability resides almost entirely in the sequential context: removing autoregressive history drops accuracy by 55.5 percentage points, while no individual feature contributes more than 0.2 pp. Cross-platform validation confirms that models are specific to both the chromatographic method and the polarity acquisition mode, but generalize perfectly across mass spectrometers sharing these parameters. The

practical consequence is that cold-start inference works immediately on new samples with no QC conditioning protocol, and a single model can serve an entire laboratory running the same analytical method. These results lay the foundation for predictive MS/MS acquisition—pre-configuring fragmentation parameters for features before they elute—which could substantially improve the annotation coverage that currently limits untargeted metabolomics.

Acknowledgments

The authors thank the Metabolomics Workbench (supported by NIH grant U2C-DK119886) for providing access to public datasets ST000983, ST000990, and ST003514. Training and transfer-learning computations were performed on Google Colab using NVIDIA Tesla T4, L4, and A100 GPUs. The clinical lipidomics data were generated by the West Coast Metabolomics Center at the University of California, Davis.

Data Availability

All code, trained model checkpoints, and processed feature tables are available in a dedicated public repository at <https://github.com/dayanjan/elution-sequence-prediction>. A GPU-ready Google Colab notebook that reproduces the transfer-learning recovery experiment is included in that repository. Publicly available mass spectrometry data were obtained from the Metabolomics Workbench: ST000983 and ST000990 (project DOI 10.21228/M8T68F)¹¹ and ST003514 (project DOI 10.21228/M8JK0Q).⁵⁵ The clinical lipidomics feature tables derived from the four plasma cohorts are available from the corresponding author on reasonable request under an appropriate data-use agreement, consistent with the governing IRB approvals and patient-consent terms for these banked human specimens.

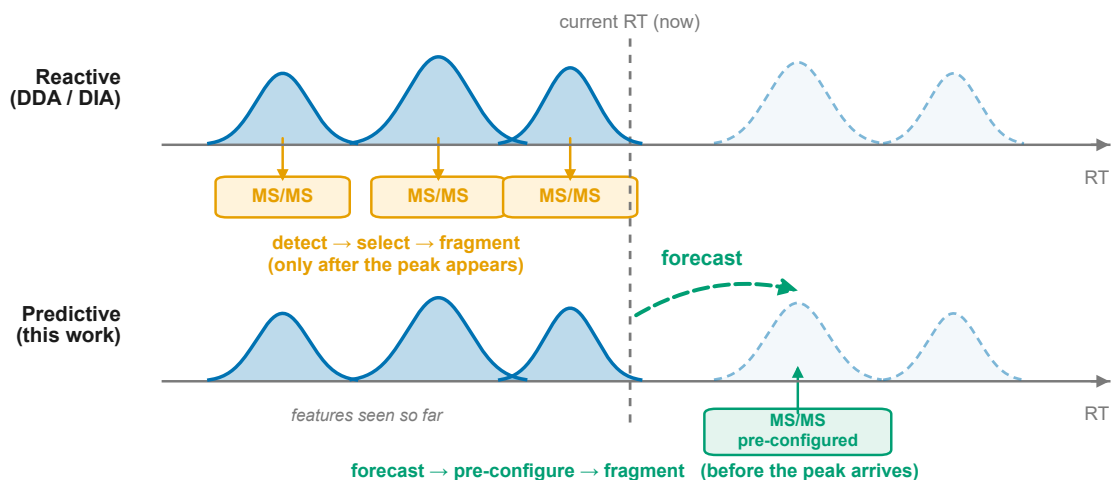
Author Contributions

Dayanjan S. Wijesinghe: Conceptualization, Methodology, Software, Formal Analysis, Investigation, Data Curation, Writing — Original Draft, Writing — Review & Editing, Visualization, Supervision, Project Administration, Funding Acquisition.

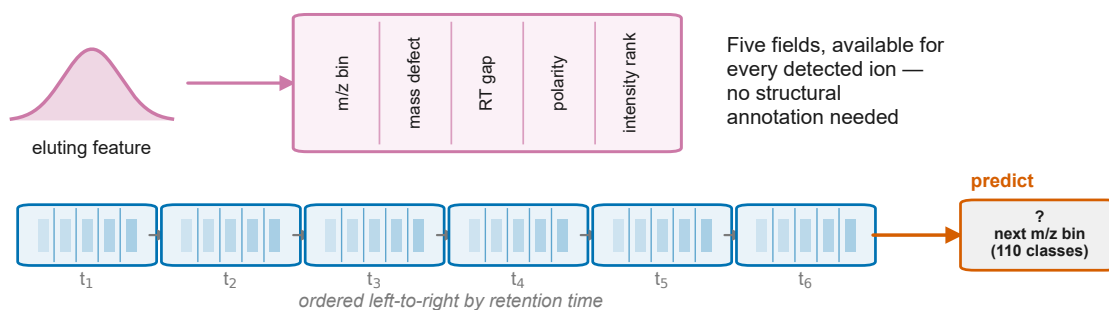
Competing Interests

The authors declare no competing interests.

A Reactive vs. predictive acquisition



B Tokenization: each feature → a 5-field token



C Study design

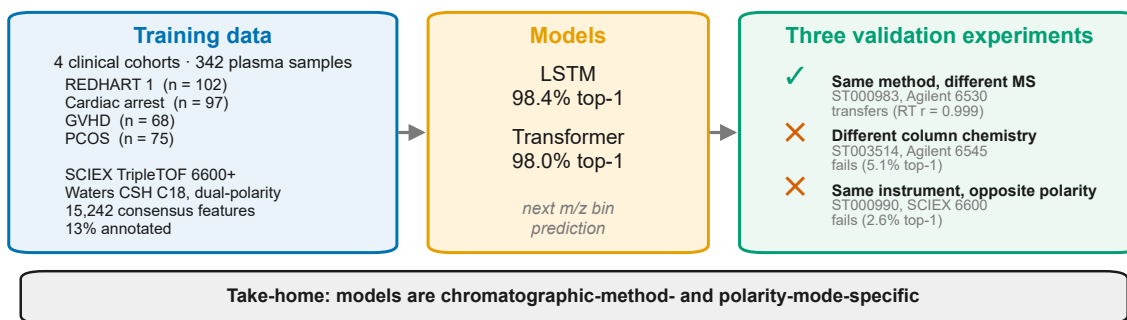


Figure 1: **Study overview.** (A) Current LC-MS/MS acquisition is reactive: the instrument detects ions, then selects precursors for fragmentation. Predictive acquisition would forecast upcoming features before they elute, enabling pre-configured MS/MS parameters. (B) Tokenization scheme. Each detected feature is encoded as a composite token with five input fields derived from the feature table, none of which require structural annotation. Features are ordered by retention time within each sample to form an elution sequence. (C) Study design. Models were trained on 15,242 consensus features from four clinical lipidomics cohorts (342 samples) and validated across three external datasets that systematically vary instrument platform and chromatographic method.

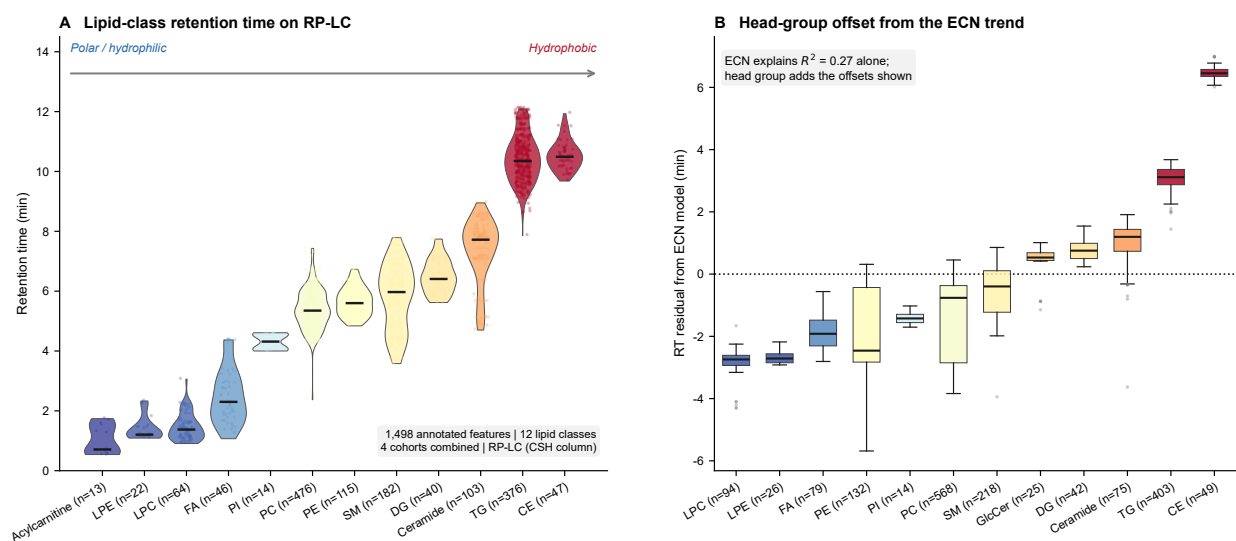


Figure 2: Physicochemical basis of elution order in reversed-phase lipidomics. (A) Retention time distributions for 12 lipid classes across all four training cohorts ($n = 1,498$ annotated features). Classes are ordered from most polar (acylcarnitine, left) to most hydrophobic (cholesteryl ester, right). Horizontal bar indicates median; individual points are jittered within each violin. Note the extensive overlap between PC, PE, and SM in the 4–7 min region. (B) Systematic head group contribution to retention time. Boxplots show residuals from a global linear model of RT vs. equivalent carbon number (ECN), grouped by lipid class ($n = 1,752$). Polar head groups (LPC, FA, LPE) elute earlier than ECN predicts; nonpolar structures (TG, CE) elute later. The span from LPC (−169 s) to CE (+389 s) confirms that head group identity introduces systematic RT offsets of up to 9.6 min at the same ECN.

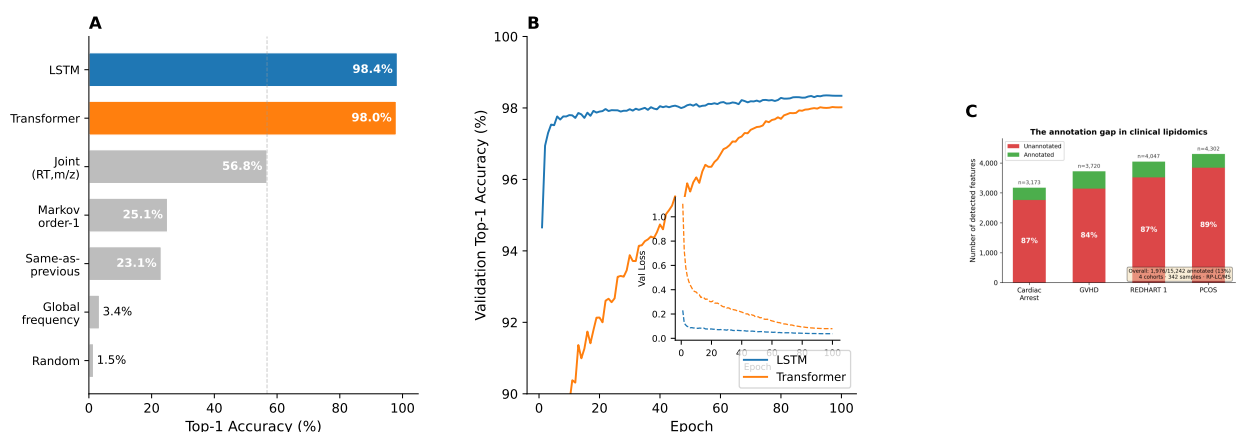


Figure 3: Model performance and dataset context. (A) Top-1 accuracy on next- m/z -bin prediction (110 classes, test set; neural models $n = 182,902$, baselines $n = 186,052$). The LSTM (98.38%) and Transformer (98.05%) far exceed all baselines, with the joint (RT, m/z) Markov model (56.8%) as the strongest non-neural comparator. Error bars indicate 95% bootstrap confidence intervals. (B) Training dynamics. Validation top-1 accuracy (solid) and validation loss (dashed) over 100 epochs for both architectures. The LSTM converges to a slightly higher asymptote; both models show an overall downward validation-loss trend with no overfitting. (C) Annotation gap across the four training cohorts. Each bar shows the number of detected features, colored by annotation status. Overall, only 13% of 15,242 consensus features received structural annotations, leaving 87% as the “dark lipidome.” Annotation rates are consistent across cohorts (10.7–15.5%), indicating a workflow-level limitation.

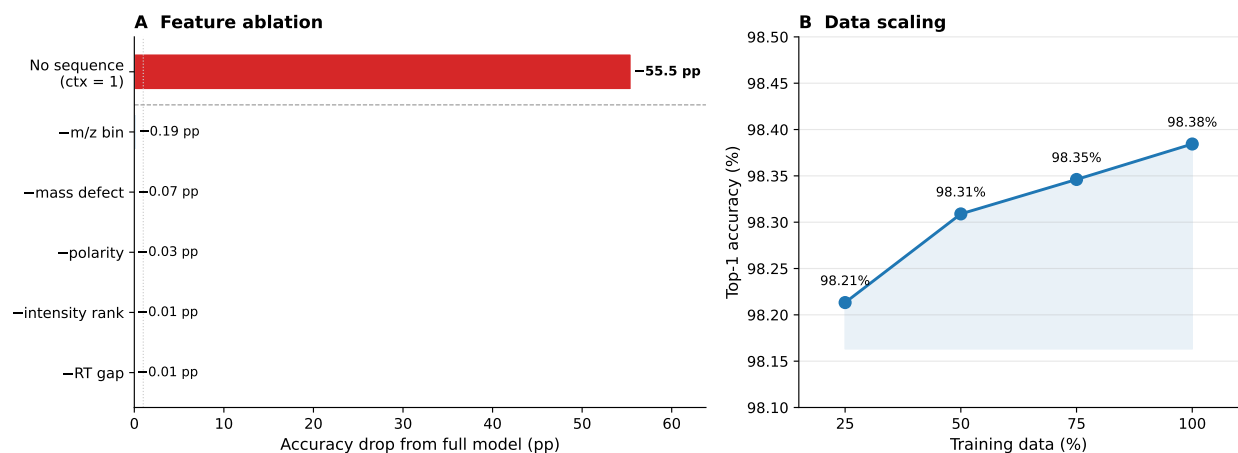


Figure 4: Feature ablation and data efficiency. (A) Accuracy drop from the full model when each input feature is removed via embedding zeroing (blue bars) or when autoregressive context is eliminated (red bar, context window = 1 token). Removing sequence context causes a 55.5 percentage-point drop; no individual feature contributes more than 0.19 pp. (B) Data efficiency curve. Top-1 accuracy as a function of training set size (25%, 50%, 75%, 100%). Performance plateaus rapidly, with 25% of data sufficient to achieve 98.2% accuracy.

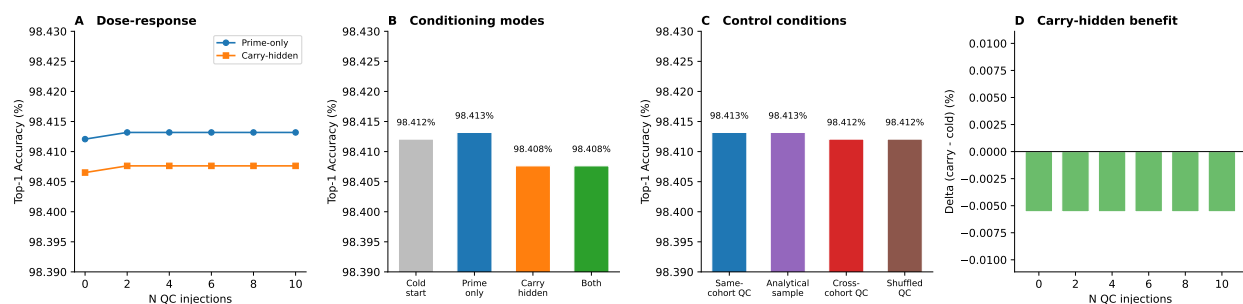


Figure 5: QC warm-up experiment: a null result. (A) Dose–response analysis. Top-1 accuracy as a function of the number of QC injection sequences used to condition the LSTM hidden state before evaluation ($N = 0–10$). The curve is flat, with no benefit from additional QC conditioning (maximum delta = 0.001%). (B) Comparison of four conditioning modes: cold start, prime-only (use QC-conditioned hidden state for first prediction only), carry-hidden (propagate hidden state through entire sample), and both. All conditions produce statistically indistinguishable accuracy. (C) Control conditions: conditioning on same-cohort QC, an analytical sample, cross-cohort QC, or order-shuffled QC injections all yield indistinguishable accuracy ($\sim 98.41\%$), confirming the null result is robust to the type of priming data. (D) Carry-hidden benefit: the accuracy delta (carry-hidden minus cold start) as a function of the number of QC injections fluctuates around zero (within $\pm 0.01\%$), confirming the absence of a warm-up benefit.

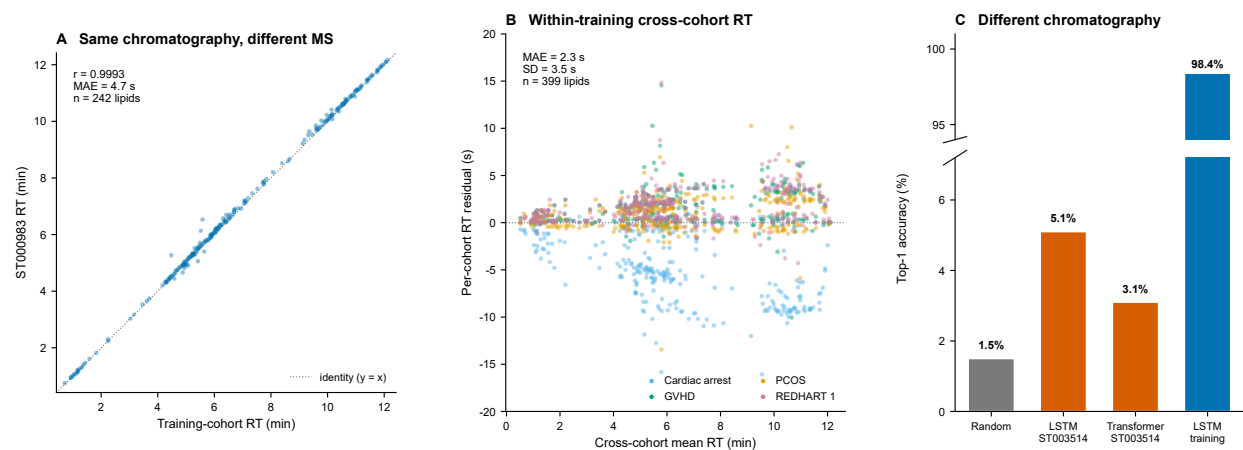


Figure 6: Cross-platform validation: models are chromatographic-method-specific. (A) Retention time correlation between the training cohorts and ST000983 (Agilent 6530 QTOF, same CSH C18 chromatographic method). Each point represents one of 242 matched lipids ($r = 0.9993$, MAE = 4.7 s). The near-perfect correlation demonstrates that elution order transfers across mass spectrometer platforms when the chromatographic method is held constant. (B) Within-training cross-cohort RT consistency: for each of 399 lipids detected in at least two training cohorts, the per-cohort median RT residual relative to that lipid’s cross-cohort mean, coloured by cohort (MAE = 2.3 s, SD = 3.5 s). Residuals cluster tightly around zero across the full elution window, demonstrating a stable elution order across independent biological cohorts (all six pairwise cohort correlations $r > 0.999$; tightest GVHD vs. REDHART 1 at $r = 1.000$; see text). (C) Model accuracy on ST003514 (Agilent 6545 QTOF, different C18 column chemistry). The LSTM achieves 5.1% and the Transformer 3.1% top-1 accuracy, near-random performance on a 110-class task, confirming that models do not transfer across chromatographic methods. The ST000990 polarity-mode failure (2.6% top-1) is described in the text.

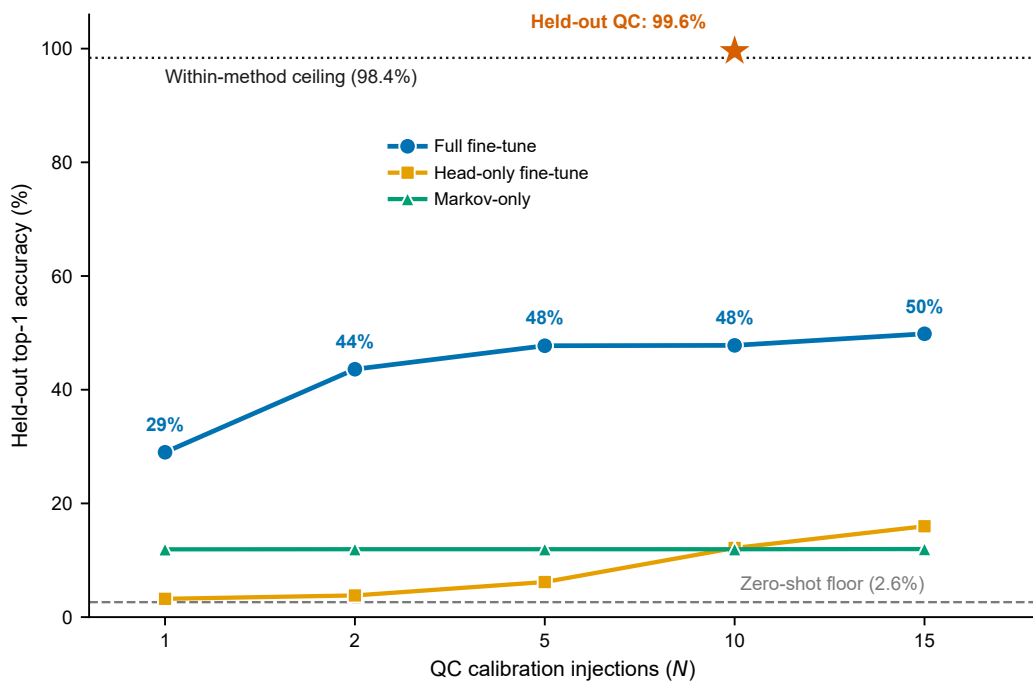


Figure 7: **Transfer learning recovers cross-polarity performance.** Held-out analytical top-1 accuracy on ST000990 (positive-ESI only) as a function of the number of QC calibration injections N , for full fine-tuning (all parameters), head-only fine-tuning (output layer only), and a calibration-only Markov prior. Full fine-tuning recovers from the 2.6% zero-shot floor (dashed) toward $\sim 50\%$ —and to 99.6% on a held-out QC injection (vermillion star)—while head-only tuning and the Markov prior plateau below 16%, localizing the cross-polarity deficit to the learned sequence representation. The dotted line is the within-method ceiling (98.4%) on matched dual-polarity data.

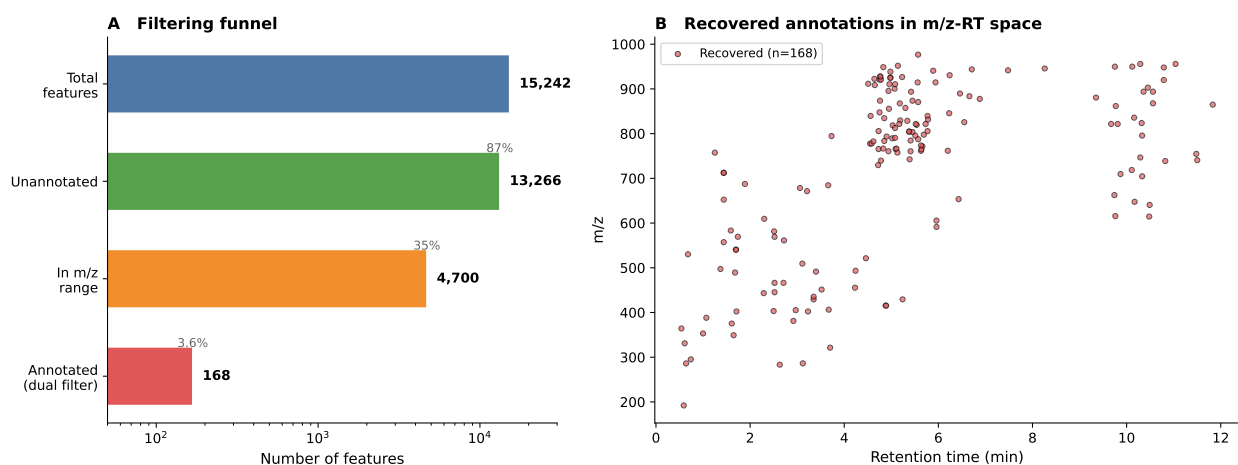


Figure 8: **Dark lipidome annotation via dual mass and retention time filtering.** (A) Filtering funnel. Of 13,266 unannotated consensus features, approximately 4,700 fell within the m/z range covered by the LipidMaps and LipidBlast reference databases. Dual filtering (± 10 ppm mass tolerance, ± 0.5 min RT tolerance) recovered 168 unique putative lipid annotations. (B) Distribution of recovered annotations (colored points) overlaid on all unannotated features (gray) in m/z -RT space. Recovered annotations span the full chromatographic range, indicating that the approach is not biased toward a specific elution region or mass range.

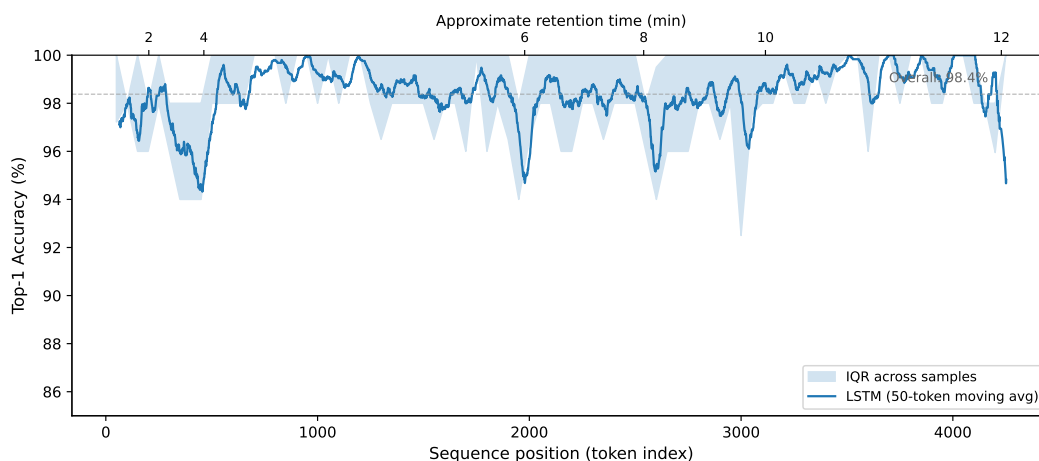


Figure 9: **Position-dependent prediction accuracy.** Top-1 accuracy on next- m/z -bin prediction as a function of sequence position (token index within the chromatographic run) for the LSTM (blue line), averaged across all test samples with a 50-token moving average. Accuracy is approximately 98% and uniform across the entire run, with no systematic degradation at early positions (where the context window is not yet fully populated) or late positions (where rare late-eluting species predominate). The shaded region indicates the interquartile range across test samples. This uniformity argues against position-specific memorization and supports the interpretation that the model learns generalizable sequential dependencies.

References

- [1] Oswald Quehenberger, Aaron M Armando, Alex H Brown, et al. Lipidomics reveals a remarkable diversity of lipids in human plasma. *J Lipid Res*, 51(11):3299–3305, 2010. doi: 10.1194/jlr.M009449.
- [2] Takeshi Harayama and Howard Riezman. Understanding the diversity of membrane lipid composition. *Nat Rev Mol Cell Biol*, 19(5):281–296, 2018. doi: 10.1038/nrm.2017.138.
- [3] Erdinc Sezgin, Ilya Levental, Satyajit Mayor, and Christian Eggeling. The mystery of membrane organization: composition, regulation and roles of lipid rafts. *Nat Rev Mol Cell Biol*, 18(6):361–374, 2017. doi: 10.1038/nrm.2017.16.
- [4] James A. Olzmann and Pedro Carvalho. Dynamics and functions of lipid droplets. *Nat Rev Mol Cell Biol*, 20(3):137–155, 2019. doi: 10.1038/s41580-018-0085-z.
- [5] Edward A. Dennis and Paul C. Norris. Eicosanoid storm in infection and inflammation. *Nat Rev Immunol*, 15(8):511–523, 2015. doi: 10.1038/nri3859.
- [6] Yusuf A. Hannun and Lina M. Obeid. Sphingolipids and their metabolism in physiology and disease. *Nat Rev Mol Cell Biol*, 19(3):175–191, 2018. doi: 10.1038/nrm.2017.107.
- [7] Matthias P. Wymann and Roger Schneider. Lipid signalling in disease. *Nat Rev Mol Cell Biol*, 9(2):162–176, 2008. doi: 10.1038/nrm2335.
- [8] Peter Libby, Julie E. Buring, Lina Badimon, Göran K. Hansson, John Deanfield, Márcio S. Bittencourt, Lale Tokgözoğlu, and Eldrin F. Lewis. Atherosclerosis. *Nat Rev Dis Primers*, 5(1):56, 2019. doi: 10.1038/s41572-019-0106-z.
- [9] Todd A. Lydic and Young-Hwa Goo. Lipidomics unveils the complexity of the lipidome in metabolic diseases. *Clinical and Translational Medicine*, 7, 2018. doi: 10.1186/s40169-018-0182-9. URL <https://www.ncbi.nlm.nih.gov/pmc/articles/PMC5786598/>.
- [10] Fang Wei, Santosh Lamichhane, Matej Orešič, and Tuulia Hyötyläinen. Lipidomes in health and disease: Analytical strategies and considerations. *TrAC Trends in Analytical Chemistry*, 120:115664, 2019. doi: 10.1016/j.trac.2019.115664. URL <https://www.sciencedirect.com/science/article/pii/S0165993619303723>.
- [11] Tomas Cajka, Jennifer T. Smilowitz, and Oliver Fiehn. Validating quantitative untargeted lipidomics across nine liquid chromatography–high-resolution mass spectrometry platforms. *Anal Chem*, 89(22):12360–12368, 2017. doi: 10.1021/acs.analchem.7b03404.
- [12] Gary J. Patti, Oscar Yanes, and Gary Siuzdak. Metabolomics: the apogee of the omic trilogy. *Nat Rev Mol Cell Biol*, 13(4):263–269, 2012. doi: 10.1038/nrm3314.
- [13] Oliver Fiehn and Jayoung Kim. Metabolomics insights into pathophysiological mechanisms of interstitial cystitis. *International Neurourology Journal*, 18(3):106–114, 2014. doi: 10.5213/inj.2014.18.3.106. URL <https://www.ncbi.nlm.nih.gov/pmc/articles/PMC4180160/>.
- [14] Emma L. Schymanski, Junho Jeon, Rebekka Gulde, Kathrin Fenner, Martin Ruff, Heinz P. Singer, and Juliane Hollender. Identifying small molecules via high resolution mass spectrometry: Communicating confidence. *Environmental Science & Technology*, 48(4):2097–2098, 2014. doi: 10.1021/es5002105.
- [15] Zhiwei Zhou, Mingdu Luo, Haosong Zhang, Yandong Yin, Yuping Cai, and Zheng-Jiang Zhu. Metabolite annotation from knowns to unknowns through knowledge-guided multi-layer metabolic network-

- ing. *Nature Communications*, 13(1), 2022. doi: 10.1038/s41467-022-34537-6.
- [16] Ricardo R. da Silva, Pieter C. Dorrestein, and Robert A. Quinn. Illuminating the dark matter in metabolomics. *Proc Natl Acad Sci U S A*, 112(41):12549–12550, 2015. doi: 10.1073/pnas.1516878112.
- [17] María Eugenia Monge, James N. Dodds, Erin S. Baker, Arthur S. Edison, and Facundo M. Fernández. Challenges in identifying the dark molecules of life. *Annu Rev Anal Chem*, 12(1):177–199, 2019. doi: 10.1146/annurev-anchem-061318-114959.
- [18] Ihab Hajjar, Chang Liu, Dean P. Jones, and Karan Uppal. Untargeted metabolomics reveal dysregulations in sugar, methionine, and tyrosine pathways in the prodromal state of AD. *Alzheimers Dement (Amst)*, 12(1):e12064, 2020. doi: 10.1002/dad2.12064.
- [19] Li Chen, Wenyun Lu, Lin Wang, et al. Metabolite discovery through global annotation of untargeted metabolomics data. *Nat Methods*, 18(11):1377–1385, 2021. doi: 10.1038/s41592-021-01303-3.
- [20] Mingxun Wang, Jeremy J. Carver, Vanessa V. Phelan, Laura M. Sanchez, Neha Garg, Yao Peng, et al. Sharing and community curation of mass spectrometry data with Global Natural Products Social Molecular Networking. *Nat Biotechnol*, 34(8):828–837, 2016. doi: 10.1038/nbt.3597.
- [21] Hisayuki Horai, Masanori Arita, Shigehiko Kanaya, et al. MassBank: a public repository for sharing mass spectral data for life sciences. *J Mass Spectrom*, 45(7):703–714, 2010. doi: 10.1002/jms.1777.
- [22] Kai Dührkop, Markus Fleischauer, Marcus Ludwig, et al. SIRIUS 4: a rapid tool for turning tandem mass spectra into metabolite structure information. *Nat Methods*, 16(4):299–302, 2019. doi: 10.1038/s41592-019-0344-8.
- [23] Kai Dührkop, Louis-Félix Nothias, Markus Fleischauer, et al. Systematic classification of unknown metabolites using high-resolution fragmentation mass spectra. *Nat Biotechnol*, 39(4):462–471, 2021. doi: 10.1038/s41587-020-0740-8.
- [24] Florian Huber, Sven van der Burg, Justin J. J. van der Hooft, and Lars Ridder. MS2DeepScore: a novel deep learning similarity measure to compare tandem mass spectra. *J Cheminform*, 13(1):84, 2021. doi: 10.1186/s13321-021-00558-4.
- [25] Felicity Allen, Allison Pon, Michael Wilson, Russ Greiner, and David Wishart. CFM-ID: a web server for annotation, spectrum prediction and metabolite identification from tandem mass spectra. *Nucleic Acids Res*, 42(W1):W94–W99, 2014. doi: 10.1093/nar/gku436.
- [26] Paolo Bonini, Tobias Kind, Hiroshi Tsugawa, Dinesh Kumar Barupal, and Oliver Fiehn. Retip: Retention time prediction for compound annotation in untargeted metabolomics. *Analytical Chemistry*, 92(11):7515–7522, 2020. doi: 10.1021/acs.analchem.9b05765. URL <https://pubs.acs.org/doi/10.1021/acs.analchem.9b05765>.
- [27] Robin Schmid, Steffen Heuckeroth, Ansgar Korf, et al. RT-Transformer: retention time prediction for metabolite annotation to assist in metabolite identification. *Bioinformatics*, 40(3):btac084, 2024. doi: 10.1093/bioinformatics/btac084.
- [28] Michael Witting and Sebastian Böcker. Current status of retention time prediction in metabolite identification. *Journal of Separation Science*, 43(9-10):1746–1754, 2020. doi: <https://doi.org/10.1002/jssc.202000060>. URL <https://onlinelibrary.wiley.com/doi/abs/10.1002/jssc.202000060>.

- [29] Eric Bach, Emma L. Schymanski, and Juho Rousu. Joint structural annotation of small molecules using liquid chromatography retention order and tandem mass spectrometry data. *Nature Machine Intelligence*, 4(12):1224–1237, 2022. doi: 10.1038/s42256-022-00577-2.
- [30] Fang-Yuan Sun, Ying-Hao Yin, Hui-Jun Liu, Lu-Na Shen, Xiu-Lin Kang, Gui-Zhong Xin, Li-Fang Liu, and Jia-Yi Zheng. Roasmi: accelerating small molecule identification by repurposing retention data. *Journal of Cheminformatics*, 17(1), 2025. doi: 10.1186/s13321-025-00968-8.
- [31] Emmanuel Defossez, Julien Bourquin, Stephan von Reuss, Sergio Rasmann, and Gaétan Glauser. Eight key rules for successful data-dependent acquisition in mass spectrometry-based metabolomics. *Mass Spectrometry Reviews*, 42(1):131–143, 2021. doi: 10.1002/mas.21715.
- [32] Hanane El Boudlali, Laura Lehmicke, and Uta Ceglarek. High-resolution accurate mass- mass spectrometry based- untargeted metabolomics: Reproducibility and detection power across data-dependent acquisition, data-independent acquisition, and acquirex. *Computational and Structural Biotechnology Journal*, 27:2412–2423, 2025. doi: 10.1016/j.csbj.2025.05.046.
- [33] Brianna T. Cooper, Ruohong Yang, et al. An assessment of acquirex and compound discoverer software 3.3 for non-targeted metabolomics. *Scientific Reports*, 2024. doi: 10.1038/s41598-024-55356-3.
- [34] Joe Wandy, Vinny Davies, Ross McBride, Stefan Weidt, Simon Rogers, and Rónán Daly. Vimms 2.0: A framework to develop, test and optimise fragmentation strategies in lc-ms metabolomics. *Journal of Open Source Software*, 7(71):3990, 2022. doi: 10.21105/joss.03990.
- [35] Kyowon Jeong, Author Corresponding, et al. Flashida enables intelligent data acquisition for top-down proteomics to boost proteoform identification counts. *Nature Communications*, 13:4407, 2022. doi: 10.1038/s41467-022-31922-z.
- [36] Christoph Wichmann, Florian Meier, Sebastian Virreira Winter, Andreas-David Brunner, Jürgen Cox, and Matthias Mann. Maxquant.live enables global targeting of more than 25,000 peptides. *Molecular & Cellular Proteomics*, 18(5):982a–994, 2019. doi: 10.1074/mcp.tir118.001131.
- [37] Brandon Bills, William D. Barshop, Seema Sharma, Jesse Canterbury, Aaron M. Robitaille, Michael Goodwin, Michael W. Senko, and Vlad Zabrouskov. Novel real-time library search driven data acquisition strategy for identification and characterization of metabolites. *Analytical Chemistry*, 94(9): 3749–3755, 2022. doi: 10.1021/acs.analchem.1c04336.
- [38] Lilian R. Heil, Philip M. Remes, Jesse D. Canterbury, Ping Yip, William D. Barshop, Christine C. Wu, and Michael J. MacCoss. Dynamic data-independent acquisition mass spectrometry with real-time retrospective alignment. *Analytical Chemistry*, 95(32):11854–11858, 2023. doi: 10.1021/acs.analchem.3c00903.
- [39] Jake B. White, Paul J. Trim, Thalia Salagaras, Aaron Long, Peter J. Psaltis, Johan W. Verjans, and Marten F. Snel. Equivalent carbon number and interclass retention time conversion enhance lipid identification in untargeted clinical lipidomics. *Analytical Chemistry*, 94(8):3476–3484, 2022. doi: 10.1021/acs.analchem.1c03770.
- [40] Zuzana Vaňková, Ondřej Peterka, Michaela Chocholoušková, Denise Wolrab, Robert Jirásko, and Michal Holčápek. Retention dependences support highly confident identification of lipid species in human plasma by reversed-phase uhplc/ms. *Analytical and Bioanalytical Chemistry*, 414(1):319–331,

2021. doi: 10.1007/s00216-021-03492-4.
- [41] Eric Bach, Sandor Szedmak, Céline Brouard, Shenghuo Liang, and Juho Rousu. Liquid-chromatography retention order prediction for metabolite identification. *Bioinformatics*, 34(17):i875–i883, 2018. doi: 10.1093/bioinformatics/bty590.
- [42] Jan Stanstrup, Steffen Neumann, and Urska Vrhošek. PredRet: Prediction of retention time by direct mapping between multiple chromatographic systems. *Analytical Chemistry*, 87(18):9421–9428, 2015. doi: 10.1021/acs.analchem.5b02287.
- [43] Álvaro González-Domínguez, Núria Estanyol-Torres, Carl Brunius, Rikard Landberg, and Raúl González-Domínguez. Qcomics: Recommendations and guidelines for robust, easily implementable and reportable quality control of metabolomics data. *Analytical Chemistry*, 96(3):1064–1072, 2024. doi: 10.1021/acs.analchem.3c03660.
- [44] Ashish Vaswani, Noam Shazeer, Niki Parmar, Jakob Uszkoreit, Llion Jones, Aidan N Gomez, Łukasz Kaiser, and Illia Polosukhin. Attention is all you need. In *Advances in Neural Information Processing Systems*, volume 30, pages 6000–6010, 2017. doi: 10.48550/arXiv.1706.03762.
- [45] Alexander Rives, Joshua Meier, Tom Sercu, Siddharth Goyal, Zeming Lin, Jason Liu, Demi Guo, Myle Ott, C. Lawrence Zitnick, Jerry Ma, and Rob Fergus. Biological structure and function emerge from scaling unsupervised learning to 250 million protein sequences. *Proc Natl Acad Sci U S A*, 118(15):e2016239118, 2021. doi: 10.1073/pnas.2016239118.
- [46] Philippe Schwaller, Teodoro Laino, Théophile Gaudin, Peter Bolgar, Christopher A. Hunter, Costas Bekas, and Alpha A. Lee. Molecular Transformer: A model for uncertainty-calibrated chemical reaction prediction. *ACS Cent Sci*, 5(9):1572–1583, 2019. doi: 10.1021/acscentsci.9b00576.
- [47] Nicholas R. Lewis, Yicheng Jin, Xiuyu Tang, Vidit Shah, Christina Doty, Bethany E. Matthews, Sarah Akers, and Steven R. Spurgeon. Forecasting of in situ electron energy loss spectroscopy. *npj Computational Materials*, 8(1), 2022. doi: 10.1038/s41524-022-00940-2.
- [48] Roman Bushuiev, Anton Bushuiev, Raman Samusevich, Corinna Brungs, Josef Sivic, and Tomáš Pluskal. Self-supervised learning of molecular representations from millions of tandem mass spectra using DreaMS. *Nat Biotechnol*, 2025. doi: 10.1038/s41587-025-02663-3. Online ahead of print.
- [49] Gabriel Asher, Mimoun Cadosh Delmar, Jennifer M. Campbell, Jack Geremia, and Timothy Kassis. LSM1-MS2: A foundation model for MS/MS, encompassing chemical property predictions, search and de novo generation, 2024. ChemRxiv preprint.
- [50] Leon L. Xu and Hannes L. Röst. Peak detection on data independent acquisition mass spectrometry data with semisupervised convolutional transformers, 2020. arXiv:2010.13841.
- [51] Hiroshi Tsugawa, Tomas Cajka, Tobias Kind, Yan Ma, Brendan Higgins, Kazutaka Ikeda, Mitsuhiro Kanazawa, Jean VanderGheynst, Oliver Fiehn, and Masanori Arita. MS-DIAL: data-independent MS/MS deconvolution for comprehensive metabolome analysis. *Nat Methods*, 12(6):523–526, 2015. doi: 10.1038/nmeth.3393.
- [52] Benjamin W Van Tassel, Justin M Canada, Salvatore Carbone, et al. Interleukin-1 blockade in recently decompensated systolic heart failure: Results from REDHART. *Circ Heart Fail*, 10(11):e004373, 2017. doi: 10.1161/CIRCHEARTFAILURE.117.004373.

- [53] Daniel Jr Contaifer, Leo F Buckley, George Wohlford, Naren Gajenthra Kumar, Joshua M Morriss, Asanga D Ranasinghe, Salvatore Carbone, Justin M Canada, Cory Trankle, Antonio Abbate, Benjamin W Van Tassell, and Dayanjan S Wijesinghe. Metabolic modulation predicts heart failure tests performance. *PLoS One*, 14(6):e0218153, 2019. doi: 10.1371/journal.pone.0218153.
- [54] Daniel Jr Contaifer, Catherine H Roberts, Naren Gajenthra Kumar, Ramesh Natarajan, others, and Dayanjan S Wijesinghe. A preliminary investigation towards the risk stratification of allogeneic stem cell recipients with respect to the potential for development of GVHD via their pre-transplant plasma lipid and metabolic signature. *Cancers (Basel)*, 11(4):466, 2019. doi: 10.3390/cancers11081051.
- [55] Sara Martínez, Miguel Fernández-García, Sara Londoño-Osorio, Coral Barbas, and Ana Gradillas. Highly reliable LC-MS lipidomics database for efficient human plasma profiling based on NIST SRM 1950. *J Lipid Res*, 65(11):100671, 2024. doi: 10.1016/j.jlr.2024.100671.
- [56] John A Bowden, Alan Heckert, Candice Z Ulmer, Christina M Jones, Jeremy P Koelmel, Laila Abdullah, Linda Ahonen, et al. Harmonizing lipidomics: NIST interlaboratory comparison exercise for lipidomics using SRM 1950-metabolites in frozen human plasma. *J Lipid Res*, 58(12):2275–2288, 2017. doi: 10.1194/jlr.M079012.
- [57] David Broadhurst, Royston Goodacre, Stacey N. Reinke, Julia Kuligowski, Ian D. Wilson, Matthew R. Lewis, and Warwick B. Dunn. Guidelines and considerations for the use of system suitability and quality control samples in mass spectrometry assays applied in untargeted clinical metabolomic studies. *Metabolomics*, 14(5):72, 2018. doi: 10.1007/s11306-018-1367-3.
- [58] H. Paul Benton, Julijana Ivanisevic, Nathaniel G. Mahieu, Michael E. Kurczy, Caroline H. Johnson, Lauren Franco, Duane Rinehart, Elizabeth Valentine, Harsha Gowda, Baljit K. Ubhi, Ralf Tautenhahn, Andrew Gieschen, Matthew W. Fields, Gary J. Patti, and Gary Siuzdak. Autonomous metabolomics for rapid metabolite identification in global profiling. *Analytical Chemistry*, 87(2):884–891, 2015. doi: 10.1021/ac5025649.
- [59] Connor Beveridge, Sanjay Iyer, Caitlin E. Randolph, Matthew Muhoberac, Palak Manchanda, and Gaurav Chopra. Claw-mrm: Comprehensive lipidomics automation workflow for multiple reaction monitoring using large language models. *Analytical Chemistry*, 2025. doi: 10.1021/acs.analchem.4c05039.
- [60] Gustav K. Reder, E. Yves Bjurstrom, Daniel Brunnsaker, Fanny Kronstrom, Paul Lasin, Ievgeniia Tiukova, Otto I. Savolainen, James N. Dodds, Jody C. May, John P. Wikswa, John A. McLean, and Ross D. King. Autonomos: Automated ion mobility metabolomic fingerprinting. *Journal of the American Society for Mass Spectrometry*, 35(3):542–550, 2024. doi: 10.1021/jasms.3c00396.
- [61] Wout Bittremieux and William Stafford Noble. Self-supervised learning from small-molecule mass spectrometry data. *Nat Biotechnol*, 2025. doi: 10.1038/s41587-025-02677-x. Online ahead of print.
- [62] Hantao Qiang, Fei Wang, Wenyun Lu, Xi Xing, Hahn Kim, et al. Language model-guided anticipation and discovery of mammalian metabolites. *Nature*, 2026. doi: 10.1038/s41586-025-09969-x.